CHALMERS

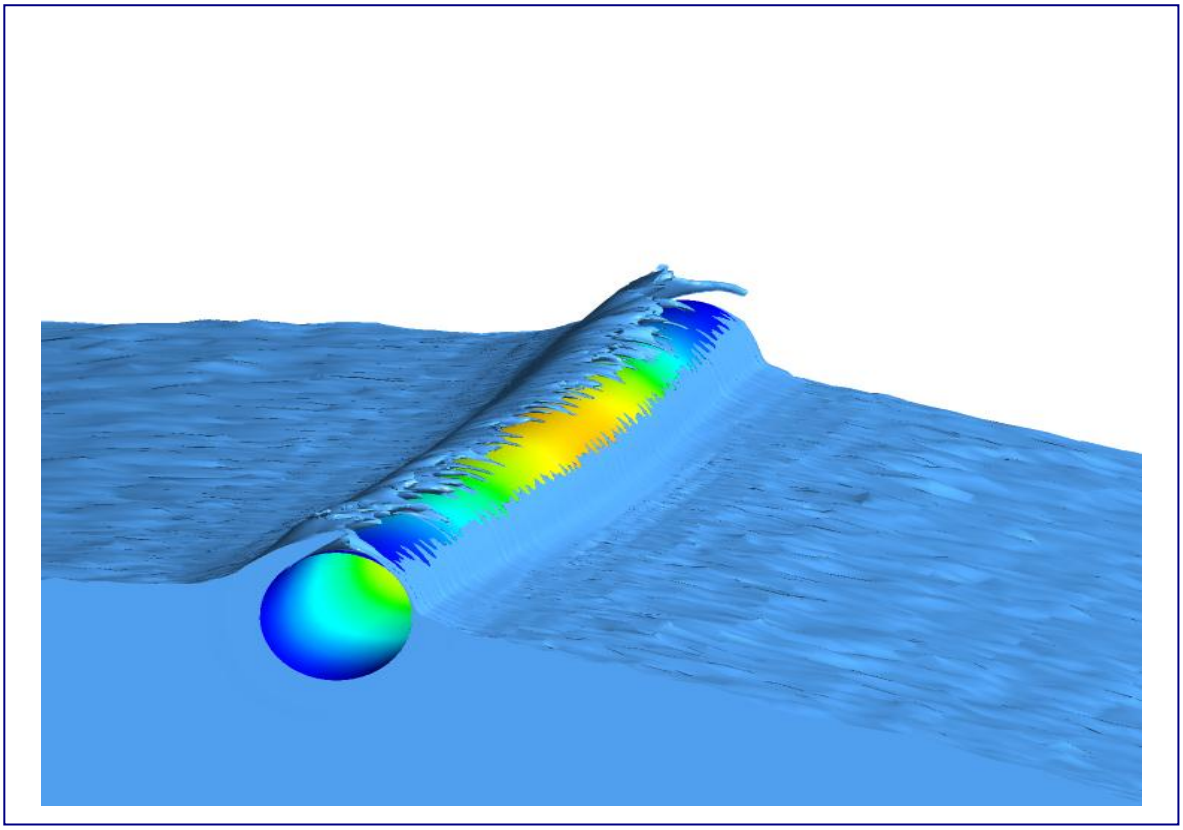

Coupled fluid structure interaction analysis on a cylinder exposed to ocean wave loading

Master's Thesis in Solid and Fluid Mechanics

RAMMOHAN SUBRAMANIA RAJA

Department of Applied Mechanics
Division of Fluid mechanics
CHALMERS UNIVERSITY OF TECHNOLOGY
Göteborg, Sweden 2012
Master's thesis 2012:55

MASTER'S THESIS IN SOLID AND FLUID MECHANICS

Coupled fluid structure interaction analysis on a cylinder exposed to ocean wave loading

RAMMOHAN SUBRAMANIA RAJA

Department of Applied Mechanics
Division of Fluid mechanics
CHALMERS UNIVERSITY OF TECHNOLOGY
Göteborg, Sweden 2012

Coupled fluid structure interaction analysis on cylinder exposed to ocean wave loading

RAMMOHAN SUBRAMANIA RAJA

Master's Thesis 2012:55
ISSN 1652-8557
Department of Applied Mechanics
Division of Fluid mechanics
Chalmers University of Technology
SE-412 96 Göteborg
Sweden
Telephone: + 46 (0)31-772 1000

Cover: Iso-surface of wave hitting the cylinder, using CFD-post.

Chalmers Reproservice
Göteborg, Sweden 2012

Coupled fluid structure interaction analysis on cylinder exposed to ocean wave loading
Master's Thesis in Solid and Fluid Mechanics
RAMMOHAN SUBRAMANIA RAJA
Department of Applied Mechanics
Division of Fluid mechanics
Chalmers University of Technology

ABSTRACT

This thesis work deals with fluid structure interaction (FSI), one of the emerging areas of numerical simulation and calculation. FSI occurs when the flow of fluid influences the properties of a structure or vice versa. It is a great challenge to deal with such problems due to its complexity in defining the geometries, nature of interaction between a fluid and solid, multi-physics facts and requirements of computational resources. This kind of interaction occurs in a wide spectrum of engineering problems and as such remains a main attraction of engineering profession.

In this thesis, the FSI analysis has been conducted on a typical slender cylindrical structural member used either as a brace or leg of an offshore truss structure. The supporting members of the structure (near to the free surface of the water) are subjected, more dominantly, to wave induced loads. Gradually, this interaction leads to the fatigue of existing structures. In 2009, a numerical study was conducted to predict the wave-in-deck load due to extreme waves on jacket platform near to free surface of the water [1]. The recent developments in numerical abilities provide easier ways to do this analysis. Here, the analysis has been approached using the partitioned method in which two ways of coupling (one-way and two-way) have been applied to simulate this cylindrical member subjected to ocean wave loads.

The fluid and structural model have been created with appropriate dimensions. ANSA [3] is used as a pre-processing tool for creating the whole computational domain and volume mesh. In order to model the non-linear high amplitude ocean wave, fifth order Stokes wave theory is used in ANSYS Fluent [4]. For the structural model, ANSYS Mechanical (transient structural) is used to determine the dynamic response of a structure under unsteady wave loads. The free surface of the water phase is tracked by using the volume of fluid (VOF) technique in Fluent. The two solvers (ANSYS Fluent & Mechanical) are coupled (exchange of data) using system coupling in ANSYS Workbench. In order to understand the dynamics of a structural member, modal analysis has been conducted to determine the natural frequencies and its respective mode shapes.

The differences in fluid forces acting on a structural member for both the ways of coupling have been analyzed. Also, an investigation has been done on the modes of deformation of a structural member in response to wave loads. Numerical results of wave force have been compared to results using Morison equation and theoretical slamming forces. Comparison work between two methods of coupling on combustion system has been taken as one of the references for the assessment of the two approaches [2].

Key words: FSI, Wave loads, One-way and two-way coupling, VOF, Dynamic response.

Preface

This Master's thesis project is carried out at Validus Engineering AB, Staffanstorp, Sweden as a part of Solid and Fluid Mechanics Master's programme at Chalmers University of technology, Gothenburg, Sweden. This work has been performed from May 2012 to October 2012. This report presents the results of Fluid-Structure interaction (FSI) analyses conducted on a typical structural member used in offshore platforms which is subjected to ocean waves. The entire analysis has been done using two different coupling methods of FSI.

Acknowledgement

I would like to express my sincere gratitude to the company's supervisor Mr.Björn Ullbrand, for his guidance and support throughout this work. I would also like to thank Dr.Håkan Nilsson, for being an examiner and directing the work.

I would like to acknowledge Validus Engineering AB for providing me efficient computational resources and software licences for completing this project in a successful way.

Furthermore, I would like to thank Lic.Eng.Martin Eriksson and Mr.Martin Orphanides, for their valuable assistance and contributions for this project.

Staffanstorp, October 2012

Rammohan Subramania Raja.

Nomenclature

E Young's modulus

S_f Solution of fluid domain

S_s Solution of solid domain

t_n nth time step

t_{n+1} n+1th time step

Re Reynolds Number

p Pressure

S_ϕ Source term in general transport equation

S_M Momentum source term

n Normal vector

u Velocity vector

u, v, w Velocity components in Cartesian coordinate system

L Wave length

T Wave period

η Free-surface displacement

H Wave height

k Wave number

m Mass matrix

k Stiffness matrix

$\ddot{\mathbf{u}}$ Acceleration vector

u Displacement vector

p Force vector

ω Forcing frequency

ω_n Natural frequency of the structural member

ρ Density

μ Dynamic viscosity

μ_t Turbulent viscosity

ϕ Scalar variable

Γ Diffusion coefficient

δ Kronecker delta

$\bar{\phi}$ Mean part of a variable in a turbulent flow

ϕ' Fluctuating part of a variable in a turbulent flow

σ_k *and* σ_s Turbulent Prandtl number

γ Volume fraction

λ Wave steepness coefficient

θ Wave phase angle

σ Wave angular frequency

Δt time step

x, y, z Cartesian coordinates

i, j Tensor indices

Acronyms

FSI Fluid Structure Interaction

CFD Computational Fluid Dynamics

CSM Computational Structural Mechanics

QUICK Quadratic Upstream Interpolation for Convective Kinetics scheme

RANS Reynolds Averaged Navier Stokes simulation

LES Large Eddy Simulation

CISCAM Compressive Interface Capturing scheme for Arbitrary Meshes

VOF Volume of Fluid method

DNS Direct Numerical Simulation

CV Control Volume

SWL Sea Water Level

PSD Power Spectral Density

Contents

1 Introduction

Fluid structure interaction (FSI) is a multi-physics phenomenon which occurs in a system where flow of a fluid causes a solid structure to deform which, in turn, changes the boundary condition of a fluid system. This can also happen the other way around where the structure makes the fluid flow properties to change. This kind of interaction occurs in many natural phenomena and man-made engineering systems. It becomes a crucial consideration in the design and analysis of various engineering systems. For instance, FSI simulations are conducted to avoid flutter on aircraft and turbo-machines [5], to evaluate the environmental loads and dynamic response of offshore structures [1, 6] and in many bio medical applications [7].

For the past ten years, the simulations of multi-physics problems have become more important in the field of numerical simulations and analyses. In order to solve such interaction problems, structure and fluid models i.e. equations which describe fluid dynamics and structural mechanics have to be coupled. Although fluid and solid solvers can be used to solve the respective domains, coupling i.e. interchange of results has been considered as one of the challenging tasks due to nonlinear nature of the fluid solid interface. But, technical advancements in the fields of computational fluid dynamics (CFD), computational structural mechanics (CSM) and numerical algorithms have made the numerical FSI analysis more realistic to be performed in a reasonable time frame.

In recent times, many commercial softwares are being developed and established to simulate FSI problems. Some of the companies like ANSYS, ADINA, COMSOL and CD-adapco provide efficient multi-physics softwares with versatile features.

1.1 Problem description

Offshore platform, also referred as oil platform, is a large structure used for exploration of oil and gas from beneath the seabed. This kind of structure contains all facilities needed to locate and extract oil and natural gas below the earth surface. The offshore platforms are normally supported by two kinds of structures, one is a fixed structure which extends to the sea bed, and the other one is a floating structure which floats on the water surface [8]. The type of structure is chosen on the basis of depth of water and other situational conditions.

Most of these platforms are placed in a rough sea environment; these structures are subjected to different types of environmental loads like waves, winds and ocean currents. Other loads are due to earth quake, tidal effects or ice [8]. It becomes very clear that the effects of environmental forces play a vital role in order to create durable offshore structures. So, the design and analysis of offshore structural members emerged as challenging tasks in the offshore business.

As mentioned above, offshore structures are exposed to various environmental forces, in which, wave induced load is considered as a dominating one in most cases. For instance, in the North Sea, there is a sign of raised significant wave height over the time which indicates rougher wave conditions [9]. Such variations in a wave height may lead to the deterioration of strength of the existing platforms. So, it is essential for an offshore engineer to estimate the forces generated by wave loading for the existing and future platforms to ensure safe and robust design. The wave induced loads can be estimated by modeling the waves using various techniques. In this

project the focus has been given to the estimation of the forces using numerical method of modeling the waves. Normally, it is a conventional way to use theoretical methods like Morison equation to find out the forces acting on structural members submerged in water [8]. But here, the structural member to be analyzed is placed near to the Sea Water Level (SWL) which cannot be handled by Morison equation due to free surface effects. This condition has led the numerical methods to be more precise than the former one.

This project aims at analyzing the wave structure interaction of a horizontal slender cylindrical member placed near to the free surface of the water. For instance this slender member could be used either as a brace of an offshore bridge or in the leg of offshore truss structure. In order to simulate high amplitude non-linear ocean waves, fifth order Stokes wave theory is applied in the numerical modeling. The wave forces computed using numerical modeling are compared with the forces evaluated by Morison equation and the forces due to wave impact loads using slamming coefficients. Structural response and its deformation due to these wave forces are also evaluated. This project has been approached by using the partitioned method of FSI; in which two ways of coupling are used to determine the realistic behavior of a cylindrical member.

1.2 Purpose

Nowadays, it has been observed by many geologists that platform subsidence occurs in many sea basins around the world due to hydrocarbon (oil and natural gas) exploitation [10]. This phenomenon results in the gradual process of increased depth for the offshore platforms, which may increase the likelihood of extreme waves hitting the structures near to the SWL and on the upper deck structures as well. The later condition is referred as e.g. Wave-in deck loading. Particularly, for structures with low air gap, installed 20-25 years before, may face a big threat due to this problem. There are many instances of structural damages on supporting structures of such platforms due to extreme weather conditions like hurricanes [10,11]. These circumstances have a created an awareness in offshore industries on things like structural durability and reliability and the requirements of setting a safer air gap.

The other reason is the reassessment of environmental data conditions. These reconsiderations have shown the variations in wave (crest) heights in the places like the North Sea and the Gulf of Mexico [9, 10]. These changes may be due to factors like recent severe hurricanes and the development of new analysis methods of prediction. Such reasons have resulted in the detailed analysis of structural members of offshore platforms which allows for the extension of the operational life of a platform.

1.3 Objectives

By taking the above purposes in to account, the objectives of the project are formulated as follows:

- To develop a method for the simulation of horizontal slender structural member subjected to fifth order Stokes wave loading using a two-way coupling FSI analysis.

- To investigate and quantify the differences in structural response as well as wave loading (fluid response) between one-way & two-way coupling methods.
- To evaluate the limitations of the one-way approach.

1.4 Assumptions and simplifications

The following statements are considered in order to reduce computational efforts, time and also to achieve reasonable conclusions from the project.

- The FSI analysis has been carried out on single typical member with appropriate dimensions instead of taking the whole structure in to account.
- The FSI analysis is also focused in analyzing the structural member with high deflection. But, it is difficult for a structural steel (E= 200Gpa) to achieve such a high deflection value and flexibility with the given length. So the Young's modulus of a structural member is reduced for a single case to get a higher deflection value compared to structural steel.
- The structure is considered to be fixed at both the ends because to avoid the deformation of symmetrical walls of the CFD model.
- The computational fluid model is created with the side boundaries exactly at the ends of cylinder which reduces a large amount of cells.
- Dynamic mesh: Normally, the CFD meshes are preferred to be built by hexahedral cells. But, the CFD mesh of this project is a hybrid mesh (combination of tetrahedral and prism layers). The reason for not using the hexahedral cells is it's incompatibility with the dynamic mesh which is used in the current version of ANSYS Fluent.
- Sea state condition: Even though the development of techniques for numerical wave modeling is appreciated, the wave theories used in simulating the sea environment are derived with some non-realistic assumptions. So the 5^{th} order Stokes wave is only an approximation of a real ocean wave.
- The effect of gravity and structural damping are not included in the structural model.
- Computational time: The entire analysis has been conducted on a work station with eight cores. The average time consumption for performing one-way analysis is noticed as 35 hours, on other hand two-way coupling typically consumes around 5 days. The reason for such long elapsed time is that System coupling cannot be supported through remote execution on e.g. Linux cluster.

2 Theoretical background

As described in the introduction, this thesis deals with FSI which is a combination of CFD and CSM, so it is essential to understand the basic physical principles and governing equations of these areas to interpret the various methods of FSI and results of this work. To begin with, different approaches of FSI are explained.

2.1 Types of approach

Normally, multi-physics problems are very difficult to solve by analytical methods. So they must be solved either by using numerical simulations or experiments. Advanced techniques and the availability of reputed commercial softwares in both CFD and CSM have made this numerical simulation possible. There are two different approaches for solving FSI problems using these softwares, the monolithic approach and the partitioned approach

2.1.1 Monolithic approach

In this approach, both sub problems (fluid and structure) are formulated as one combined problem. The system of algebraic equations resulted from discretization of governing equation are solved as a whole [12,13]. The interaction of fluid and structure at the interface is treated synchronously. This leads to the conservation of properties at the interface possible which increases the stability of the solution. *Figure 2-1* represents the flow process of monolithic approach.

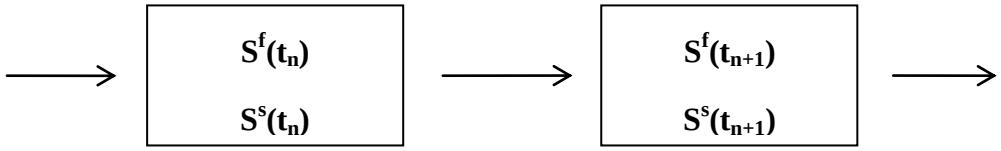

Figure 2-1 Monolithic approach

This approach is considered to be more robust than the partitioned approach. But this approach is computationally expensive and cannot take the advantage of software modularity as the partitioned method does.

2.1.2 Partitioned approach

The other choice for solving the FSI problems is the partitioned method. Here, both sub problems are solved separately which means the flow does not change while the structural solution is calculated. The equations governing the flow and the displacement of the structure are solved alternatingly in time with two distinct solvers. The intermediate fluid solution is prescribed as a boundary condition for the structure and vice versa, and the iteration continues until the convergence criterion is satisfied. At the interface (boundary between fluid and solid), the exchange of information occurs according to the type of coupling technique applied [12,13]. *Figure 2-2* explains the process of partitioned method.

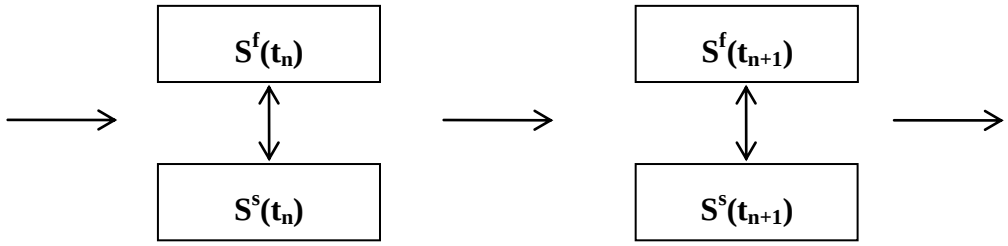

Figure 2-2 Partitioned approach

Due to the time lag between the integration of the fluid and structure domains, the interface conditions are implemented asynchronously which leads to a possibility of losing conservation of properties. But, this problem can be rectified by using mapping algorithms as given in section 2.5.2. Nevertheless, this allows the preservation of the software modularity.

As mentioned in the above paragraph, the information is exchanged at the interface between two solvers, this process is defined as the *coupling*, and this is of two types.

2.1.3 One-way coupling

The coupling is one-way if the motion of a fluid flow influences a solid structure but the reaction of a solid upon a fluid is negligible [14]. The other way around is also possible. Example: Ship propeller.

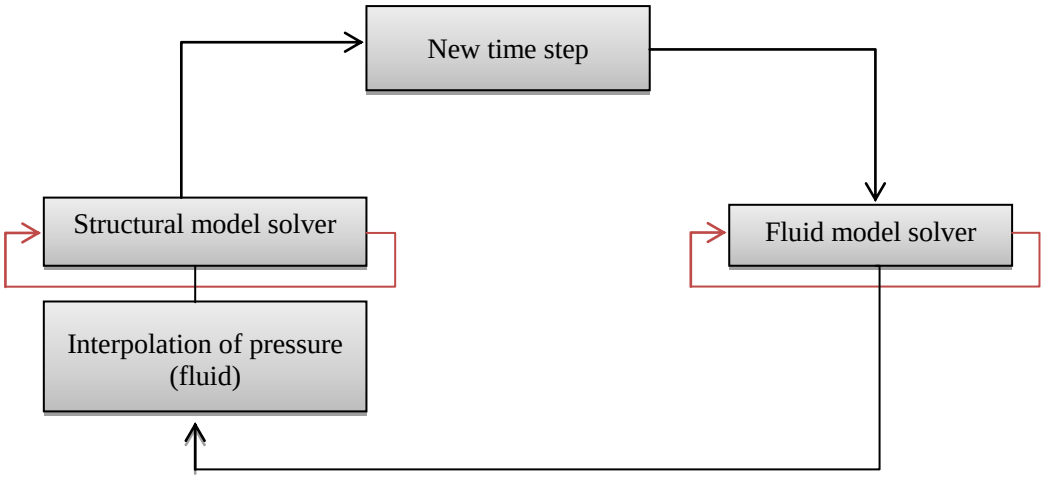

Figure 2-3 One-way coupling- flow chart

Figure 2-3 explains the one way coupling method**.** Initially, the fluid flow calculation is performed until convergence is reached. Then the resulting forces at the interface from fluid calculation are interpolated to the structural mesh. Next, the structural dynamic calculations are performed until the convergence criterion is met. This is repeated until the end time is reached.

2.1.4 Two-way coupling

This type of coupling is applied to the problem where the motion of a fluid influences a solid structure and at the same time the flow of fluid is influenced by reaction of a solid structure. Example: Wind power plant.

The work flow of the strong two-way coupling algorithm is shown in *Figure 2-4*. During the first time step, converged solutions of the fluid calculation provide the forces acting on the solid body. Then the forces are interpolated to the structural mesh like in one-way coupling and the solution from the structural solver is obtained with those fluid forces as boundary conditions. As a consequence the mesh is deformed according to the response of structure. These displacement values are interpolated to the fluid mesh which results in deformation of the fluid domain. This process is repeated until both force and displacement values are converged below the pre-determined limit [14].

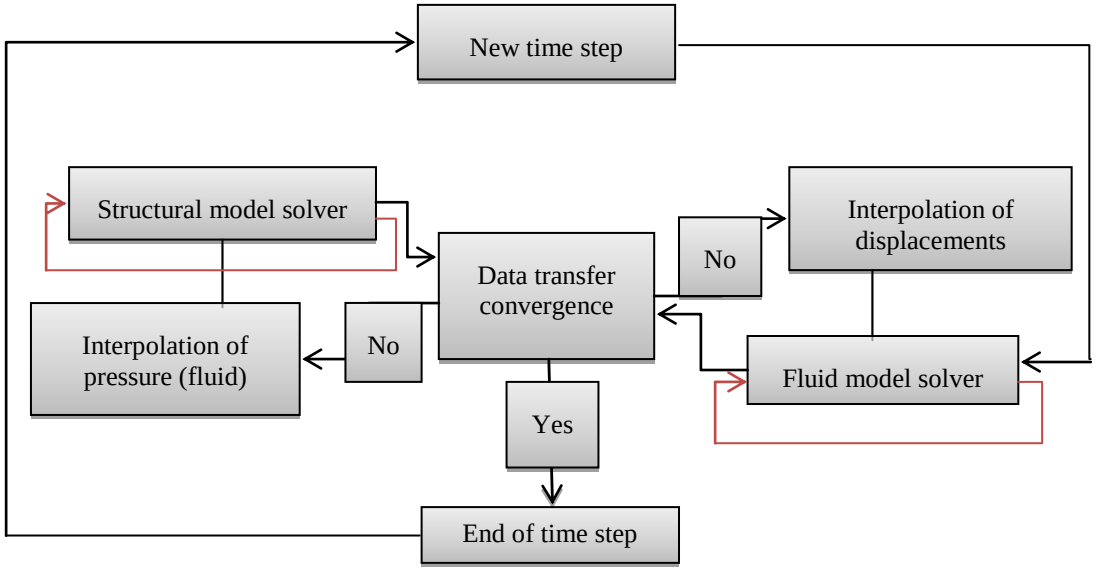

Figure 2-4 Two-way coupling- flow chart

2.2 CFD and fluid model

All kinds of fluid flow and transport phenomena are governed by basic conservation principles such as conservation of mass, momentum and energy. All these conservation principles are solved according to the fluid model which gives set of partial differential equations, called the governing equations of the fluid. The following part elaborates on the theoretical background of CFD and the way it is employed for this particular case.

2.2.1 Mass conservation principle and continuity equation

The mass conservation principle states that the rate of increase of mass in a fluid element is equal to the net rate of flow of mass into a fluid element. Applying this physical principle to a fluid model results in a differential equation called continuity

equation [15]. The continuity equation for a compressible fluid can be written as follows

$$\frac{\partial \rho}{\partial t} + div\,(\rho u) = 0 \qquad (2\text{-}1)$$

where ρ represents the density and u represents velocity of the fluid.The first term of the equation is the rate of change of density with respect to time and the next term is net flow of mass out of the element boundaries.

2.2.2 Newton's second law and momentum equation

Newton's second law states that the rate of change of momentum of a fluid particle equals to the sum of the forces acting on a particle. The forces acting on a body are a combination of both surface and body forces. When this law is applied for Newtonian fluid (viscous stress is proportional to the rates of deformation) resulting equations are called as Navier Stokes equations. The equations written below explain the momentum conservation principle [15]

$$\frac{\partial(\rho u)}{\partial t} + div\,(\rho u \mathrm{u}) = -\frac{\partial \mathrm{p}}{\partial \mathrm{x}} + div\,(\mu\, grad\ u) + S_{Mx} \qquad (2\text{-}2)$$

$$\frac{\partial(\rho v)}{\partial t} + div\,(\rho v \mathrm{u}) = -\frac{\partial \mathrm{p}}{\partial \mathrm{y}} + div\,(\mu\, grad\ v) + S_{My} \qquad (2\text{-}3)$$

$$\frac{\partial(\rho w)}{\partial t} + div\,(\rho w \mathrm{u}) = -\frac{\partial \mathrm{p}}{\partial \mathrm{z}} + div\,(\mu\, grad\ w) + S_{Mz} \qquad (2\text{-}4)$$

where ρ represents the density , u represents velocity vector, u , v , w are the velocity components in Cartesian coordinate system, μ is the dynamic viscosity and S_M represents the momentum source term. Since the problem at hand does not involve the heat transfer, energy equation is not considered.

2.2.3 Finite volume method

The finite volume method is one of the numerical techniques applied in well-established commercial CFD codes to solve the governing equations of the fluid. The basic and foremost step of CFD is dividing the computational domain (geometry of the region of interest) in to number of smaller regions called control volumes or cells and the collection of these cells is called a grid or a mesh, also, the calculated scalar values are stored at the center of the control volumes. Fluent uses the finite volume technique to convert the general transport equation in to a system of algebraic equations and it uses different iterative methods to solve the algebraic equations. The following are the key steps in order to find the solution for the transport equation of a physical quantity [15].

The steps are as follows

- Division of geometry in to smaller regions (control volumes) using a computational mesh.

- Integration of the governing equations of fluid over all the control volumes of the domain.
- Discretization – conversion of the resulting integral equations in to a system of algebraic equations.
- Finding a solution to the system of algebraic equations by an iterative method.

The general form of transport equation in conservative form can be written as [15]

$$\frac{\partial(\rho\phi)}{\partial t} + div(\rho\phi \mathrm{u}) = div(\Gamma\, grad\ \phi) + S_\phi \qquad (2\text{-}5)$$

where the variable ϕ can be replaced by any scalar quantity, Γ is the diffusion coefficient. The left hand side of the equation contains the rate of change term and convective term, whereas the diffusive term and source term lie on the right hand side of the equation. Integrating over the control volume and applying the Gauss's divergence theorem on the general transport equation gives [15]

$$\frac{\partial}{\partial t}\int_{CV}\rho\phi\, dV + \int_A n\,(\rho\phi \mathrm{u})\, dA = \int_A n\,(\Gamma\, grad\ \phi)\, dA + \int_{CV} S_\phi\, dV \qquad (2\text{-}6)$$

2.2.4 Spatial and temporal discretization schemes

The above transport equation is subjected to the stated key steps of the finite volume technique and the discretized equation for each control volume is obtained through suitable discretization schemes. There are many spatial discretization schemes for formulating diffusive and convective terms of the transport equation.

In the case of diffusive term in the discretized equation, the gradients of a variable at the faces of the control volume are required. In order to find a value of this term, a central differencing scheme is used by considering linear approximation. On the other hand, the convective term at the faces of the control volume is evaluated by using an upwind scheme. The main idea of this scheme is that convective values at the face are calculated by using the values of upstream control volume or relative to the direction of the normal velocity (u).Fluent has a range of upwind schemes such as first order upwind, second order upwind, power law and QUICK (Quadratic Upstream Interpolation for Convective Kinetics scheme) [16]. All the above discretization schemes are mainly categorized by the order of solution accuracy. Apart from this, results produced from these schemes are physically realistic when it fulfills the following properties [15].

- Conservativeness
- Boundedness
- Transportiveness

For unsteady calculations, the transport equation must be discretized in both space and time. Temporal discretization involves the integration of all terms of transport equation over a time step Δt. The two main schemes available for temporal discretization in ANSYS Fluent are implicit time integration and explicit time integration [16].

2.2.5 Turbulent flow and Turbulence modeling

Turbulent flow is a type of fluid flow characterized by fluctuating and chaotic property changes. When the Reynolds number (Re) exceeds certain limit the flow becomes turbulent, properties such as pressure and velocity changes with high frequency and continuously with time. Although Navier Stokes equation is capable of evaluating the solution by taking this turbulence in to account, it needs enormous computational resources to simulate and resolve such small scales of fluctuations. This type of approach is called as Direct Numerical Simulation (DNS). An alternative method is to employ turbulence models to model the effect of turbulence in the flow. The Reynolds Averaged Navier Stokes simulation (RANS) and Large Eddy Simulation (LES) are the two kinds of approaches which employ its own kind of Navier Stokes equation to model the turbulent flow by the use of turbulence models [17]. In this work, RANS is used to model to the effects of turbulence.

2.2.5.1 Reynolds Averaged Navier Stokes Simulation (RANS)

In this approach, the variables in Navier Stokes equation are decomposed in to mean ($\bar{\phi}$) and fluctuating (ϕ') part. This is called as Reynolds decomposition [16]. The Reynolds decomposition can be written as

$$\phi = \bar{\phi} + \phi' \qquad (2\text{-}7)$$

By substituting the flow variables of governing equation in this form will result in Reynolds Averaged Navier Stokes equation. The tensorial form of the equation in Cartesian coordinate system can be written as

$$\frac{\partial}{\partial t}(\rho u_i) + \frac{\partial}{\partial x_j}(\rho u_i u_j) = -\frac{\partial p}{\partial x_i} + \frac{\partial}{\partial x_j}\left[\mu\left(\frac{\partial u_i}{\partial x_j} + \frac{\partial u_j}{\partial x_i} - \frac{2}{3}\delta_{ij}\frac{\partial u_i}{\partial x_i}\right)\right] + \frac{\partial}{\partial x_j}(-\rho u'_i u'_j) \qquad (2\text{-}8)$$

where i, j are tensor indices and δ_{ij} is Kronecker delta.This equation is similar to the general form of the Navier Stokes equation, but this decomposition of flow variables introduced a new term on the right hand side of the equation, called Reynolds stress term, which is unknown. The main motivation of this approach is to *model* the Reynolds stresses.

Boussinesq hypothesis relates the Reynolds stresses to the mean velocity gradients [16] which is given as

$$-\rho u'_i u'_j = \mu_t\left(\frac{\partial u_i}{\partial x_j} + \frac{\partial u_j}{\partial x_i}\right) - \frac{2}{3}\left(\rho k + \mu_t \frac{\partial u_k}{\partial x_k}\right)\delta_{ij} \qquad (2\text{-}9)$$

Where μ_t is the turbulent viscosity, k is the kinetic energy. This hypothesis is used in turbulence models such as Spalart-Allmaras model, *k-ε* models and the *k-ω* models. Here, realizable *k-ε* model, one of the variants of *k-ε* models is used in turbulence modeling.

2.2.5.2 Realizable *k-ε* model

The realizable *k-ε* model is a two equation turbulence model, which holds two more additional transport equations (one for turbulent kinetic energy (k) and one for turbulence dissipation rate (ε)) which are required to be solved and the turbulent viscosity (μ_t) which is evaluated as a function of both k and ε [16]. The transport equations for k and ε in the realizable *k-ε* model are

$$\frac{\partial}{\partial t}(\rho k)+\frac{\partial}{\partial x_j}(\rho k u_j)=\frac{\partial}{\partial x_j}\left[\left(\mu+\frac{\mu_t}{\sigma_k}\right)\frac{\partial k}{\partial x_j}\right]+G_k+G_b-\rho\varepsilon-Y_M+S_k \qquad (2\text{-}10)$$

$$\frac{\partial}{\partial t}(\rho\varepsilon)+\frac{\partial}{\partial x_j}(\rho\varepsilon u_j)=\frac{\partial}{\partial x_j}\left[\left(\mu+\frac{\mu_t}{\sigma_\varepsilon}\right)\frac{\partial \varepsilon}{\partial x_j}\right]+\rho C_1 S_\varepsilon-\rho C_2\frac{\varepsilon^2}{k+\sqrt{\nu\varepsilon}}+C_{1\varepsilon}\frac{\varepsilon}{k}C_{3\varepsilon}G_b+S_\varepsilon \qquad (2\text{-}11)$$

Where $C_1=\max\left[0.43+\frac{\eta}{\eta+5}\right]$, $\eta=S\frac{k}{\varepsilon}$, $S=\sqrt{2S_{ij}S_{ij}}$

In the above equations, G_k indicates the generation of turbulence kinetic energy due to the mean velocity gradients, G_b indicates the generation of turbulence kinetic energy due to buoyancy, Y_M represents the contribution of the fluctuating dilation in compressible turbulence to the overall dissipation rate. C_2 and $C_{1\varepsilon}$ are constants, σ_k and σ_ε are the turbulent Prandtl number for k and ε respectively.

2.2.5.3 Near wall treatment

Generally, turbulent flows are affected by the presence of walls. In the near-wall region, the solution variables have large gradients; therefore an accurate representation of the flow in this region yields realistic solutions of wall bounded turbulent flows. One of the main approaches for modeling the wall bounded turbulent flow is to use set of semi empirical formulas called “wall functions” which are used to bridge the viscosity-affected region between the wall and fully turbulent region. The detailed explanation of wall functions and its variants are given in [16]. In this project, the near-wall flow is modeled using non-equilibrium wall function.

2.2.6 Multiphase Modeling and Volume of Fluid model (VOF)

This thesis work involves one of the multiphase flow regimes called free surface (gas-liquid); free surface is an interface between a liquid and a gas. The VOF method is a popular numerical technique used in detecting the free surface of the computational domain. There are two general approaches available in multiphase flow modeling such as Euler-Lagrange approach and Euler-Euler approach [16]. The first approach considers the fluid phase as a continuum and solves the Navier stokes equation, on other hand dispersed phase is solved by tracking the particles all over the flow field. The later one treats different phases as interpenetrating continua and introduces a term called phase indicator function or volume fraction.

VOF model belongs to the Euler-Euler approach, which can model two or more immiscible fluids by solving the volume averaged flow equations and tracks the volume of fraction of the fluids in the whole computational domain. In each control volume, the sum of the volume fraction of all the phases equals to one. For instance if the volume fraction of phase 1 in the cell is given as γ, then the following three cases are possible [18]

- γ = 0, this shows that the particular control volume does not contain this fluid.
- γ = 1, this shows that the control volume is entirely occupied by the fluid.
- 0 <γ< 1, this control volume contains the interface between this n^{th} fluid and other one.

Based on the value of this term γ, the properties of the flow variable are given in the volume averaged flow equations. For example, the density can be given according to the equation follows [18]

$$\rho = \gamma\rho_1 + (1-\gamma)\rho_2 \qquad (2\text{-}12)$$

The solution of the volume fraction can be estimated using the advection equation, since it is being the scalar property of a fluid. The transport equation of volume fraction (γ) can be written as [18]

$$\frac{\partial \gamma}{\partial t} + \frac{\partial u_i \gamma}{\partial x_i} = 0 \qquad (2\text{-}13)$$

Generally, the volume fraction of a primary phase is not solved; instead it is evaluated using an expression (1-γ) because the sum of volume fraction of all phases equals to unity in all control volumes.

In Fluent, the volume fraction equation can be discretized by set of time-discretization schemes such as explicit and implicit schemes. The explicit and implicit schemes treat the cells with standard interpolation (first and second order upwind, QUICK) schemes that are occupied with one phase or other. But, there are some discretization schemes which are applied to the cells near to the interface between two phases. The schemes used in Fluent are the geometric reconstruction scheme, the donor-acceptor scheme, the compressive interface capturing scheme for arbitrary meshes (CISCAM) and the compressive and zonal discretization scheme [16]. In this project work, the compressive and zonal discretization scheme is used because it is not computationally expensive.

2.3 Wave theory and modeling

Generally, offshore structures are exposed to various environmental loads which are induced by wave, wind and current. It is essential for offshore engineers to predict the forces generated by these wave loads because of its dominance compared to other environmental forces. In the following part, the techniques for modeling the waves and to determine its effects on structural members are explained.

Generally, a wave is defined as a disturbance or energy which spreads in matter or space; ocean waves or water waves propagate such disturbances through water as a medium. This is mainly generated by wind in deep oceans and these waves require

restoring forces to propagate. In most of the cases, Earth's gravity act as the major restoring force and when the wave scale is small, surface tension is sufficient to propagate the wave. In reality, ocean wave propagation is highly nonlinear; it propagates in different directions with varying wave heights and wave lengths in certain period of time. In order to determine the forces on offshore structures resulted from ocean waves it is necessary to model a prototype wave system. There are techniques like analytical wave modeling, empirical wave modeling, physical wave modeling and numerical wave modeling available to model a prototype ocean wave environment [19]. In this project, a wave model is created using the numerical technique.

2.3.1 Numerical wave modeling

A numerical wave model is a suitable representation of a prototype wave using mathematical equations. The wave equations are obtained from theoretical wave studies, which provide information about wave motion like water particle kinematics with required input parameters. It is better to understand the wave characteristic parameters before the explanation of wave theories and modeling technique to simulate the ocean waves. *Figure 2-5* depicts the common wave characteristic parameters and the definitions of the parameters [19] are given below.

SWL – still water level (y= d); d- water depth

Wave length (L): Length of a one complete cycle of a wave or distance between two successive crests/troughs in a wave.

Wave period (T): Time required for completing one wave cycle.

Wave elevation (η): Instantaneous vertical displacement of sea surface above the SWL.

Wave height (H): The distance between the elevation of a crest and its neighboring trough.

Many wave theories have been developed to model different kinds of waves with its associated level of complexity. Some of the wave theories are linear (Airy waves), Stokes second and higher order theories and cnoidal wave theories. But all these wave theories are derived with some basic assumptions for the purpose of achieving appropriate solutions [21]. The following assumptions are made to derive the wave theories.

- The sea bed is impermeable and horizontal (flat).
- The wave propagation is unidirectional.
- The flow is two-dimensional.
- The fluid is ideal i.e. inviscid, incompressible and irrotational.

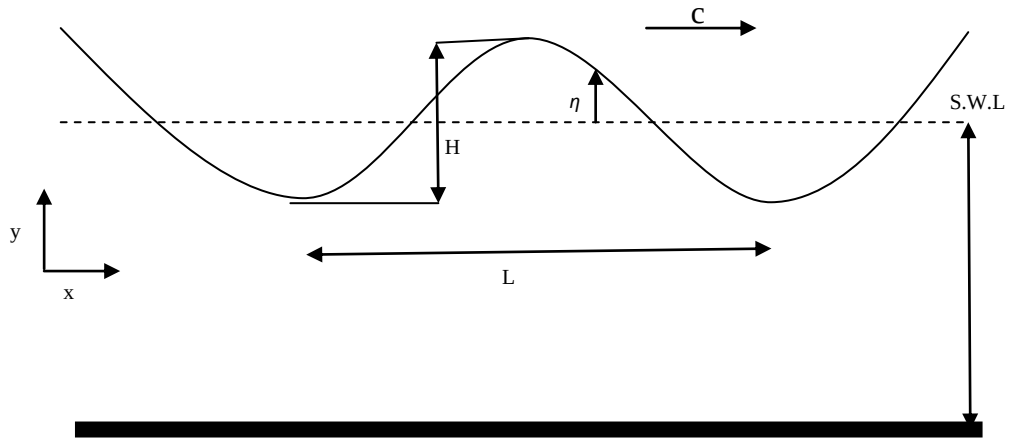

Figure 2-5 Wave characteristic parameters

The above assumptions are not matching with our problem because the flow is 3D, viscous and rotational, but stability of the solution is maintained because of short time interval of analysis. Linear wave theory is used for small amplitude waves, Stokes and cnoidal wave theories are applicable for large amplitude waves in deep and shallow waters respectively. Le Mahaute (1969) provided the detailed chart for validity range of various wave theories using water depth (d) and wave height (H). The water depth and wave height used in this project have been selected through the chart shown in *Figure 3-10*.

2.3.2 Stokes fifth order wave theory

The equations for instantaneous vertical displacement (η), wave height (H) and velocities used in fifth order Stokes wave are described below. The free surface displacement can be given as [19]

$$\eta = \sum_{i=1}^{5} a_i \cos(i\theta)$$

$$= \frac{1}{k}\left[\lambda \cos\theta + (\lambda^2 B_{22} + \lambda^4 B_{24})\cos 2\theta + (\lambda^3 B_{33} + \lambda^5 B_{35})\cos 3\theta + \lambda^4 B_{44} \cos 4\theta + \lambda^5 B_{55} \cos 5\theta\right] \quad (2\text{-}14)$$

where k is the wave number, λ is the wave steepness coefficient and θ is the phase angle. The coefficients *B* are given in Appendix 0.

The wave height and the dispersion equation are the functions of k and λ which can written as

$$H = \frac{2}{k}\left[\lambda + B_{33}\lambda^3 + (B_{35} + B_{55})\lambda^5\right] \quad (2\text{-}15)$$

$$\omega^2 = gk \tanh kh\,(1 + C_1\lambda^2 + C_2\lambda^4) \quad (2\text{-}16)$$

Newton-Raphson iteration method is used to solve the above two equations to obtain the value of k and λ for the given H, h, T. The value C_1 and C_2 are given in Appendix 0 .The expressions for the horizontal and the vertical velocities can be given as

$$\begin{aligned} u = c\{&\lambda(A_{11} + \lambda^3 A_{13} + \lambda^5 A_{15})\cosh[k(h+d)]\cos\theta \\ &+ 2(\lambda^2 A_{22} + \lambda^4 A_{24})\cosh[2k(h+d)]\cos 2\theta \\ &+ 3(\lambda^3 A_{33} + \lambda^5 A_{35})\cosh[3k(h+d)]\cos 3\theta \\ &+ 4\lambda^4 A_{44}\cosh[4k(h+d)\cos 4\theta] + 5\lambda^5 A_{55}\cosh[5k(h+d)]\cos 5\theta\} \end{aligned} \quad (2\text{-}17)$$

$$\begin{aligned} w = c\{&\lambda(A_{11} + \lambda^3 A_{13} + \lambda^5 A_{15})\sinh[k(h+z)]\sin\theta \\ &+ 2(\lambda^2 A_{22} + \lambda^4 A_{24})\sinh[2k(h+z)]\sin 2\theta \\ &+ 3(\lambda^3 A_{33} + \lambda^5 A_{35})\sinh[3k(h+z)]\sin 3\theta \\ &+ 4\lambda^4 A_{44}\sinh[4k(h+z)\sin 4\theta] + 5\lambda^5 A_{55}\sinh[5k(h+z)]\sin 5\theta\} \end{aligned} \quad (2\text{-}18)$$

The coefficients A are given in Appendix 0.

2.3.3 Morison equation

Morison equation is a semi-empirical formula used to find the forces acting on a body subjected to an oscillatory flow. This equation is a combination of both inertial force and drag force which gives the resultant force (per unit length) acting on a body as shown in the below equation [8]

$$F(t) = \frac{\pi}{4}\rho C_M D^2 \dot{u}(t) + \frac{1}{2}\rho C_D u(t)|u(t)| \quad (2\text{-}19)$$

where $F(t)$ is the horizontal force per unit length, D is the diameter of a cylinder, $u(t)$ is the wave particle velocity in horizontal direction, $\dot{u}(t)$ represents the acceleration term and C_M&C_D are the hydrodynamic coefficients. These dimensionless coefficients are determined by experiments. As explained in sec this equation is used for comparing the magnitude of horizontal forces obtained using numerical simulations.

2.3.4 Wave slamming force

The wave slamming force creates impact loads on the structural members of offshore structure. The prediction of wave slamming forces is considerably important as horizontal forces acting on structural members. The equation for finding the slamming force per unit length acting on the horizontal structural member is given as [22]

$$F_s = \frac{1}{2}\rho D C_s v^2 \quad (2\text{-}20)$$

where *v* is the wave particle velocity in vertical direction. *Cs* is the wave slamming coefficient.

2.4 Finite Element Method and structural model

In this thesis work, both transient dynamic and modal analyses have been performed to evaluate the dynamic response and vibrational characteristics of the structural member respectively. The following sub-sections are provided with the information about these types of analyses and Finite Element method (FEM).

2.4.1 Transient dynamic analysis

Structural dynamics is the study of behavior of structures under the application of loads. The project work involves the transient dynamic analysis which determines the structural response under the impulse load. The loads acting on a structure are of two types. The first type is static load which does not vary with time and gives enough time for a structure to respond, whereas, the second one called dynamic load, changes with time quickly compared to the static loads. Impulse load is a kind of dynamic load, acts on the system or structure with larger magnitude within a short interval of time. Through this analysis, the time history of responses such as displacement, stress, strain of structure can be calculated. The basic governing equation of motion for MDOF system is given as [19]

$$\mathbf{m}\ddot{\mathbf{u}} + \mathbf{c}\dot{\mathbf{u}} + \mathbf{k}\mathbf{u} = \mathbf{p}(t) \qquad (2\text{-}21)$$

where is a $\mathbf{m}$ structural mass matrix, $\ddot{\mathbf{u}}$ is an acceleration vector, $\mathbf{c}$ is a structural damping matrix, $\dot{\mathbf{u}}$ is a velocity vector, $\mathbf{k}$ is a structural stiffness matrix, $\mathbf{u}$ is a displacement vector, $\mathbf{p}$ is a force vector which is a function of time. As mentioned in section 1.4, the structural damping is not involved in the finite element model; the above governing equation is modified into following form

$$\mathbf{m}\ddot{\mathbf{u}} + \mathbf{k}\mathbf{u} = \mathbf{p}(t) \qquad (2\text{-}22)$$

It is normal practice to use a numerical technique called finite element method (FEM) to find the solution for equation (2-22), because it is not feasible to use analytical methods to determine the solution for a system with infinite number of Degrees of Freedom (DOFs). The basic principle behind this method of finding an approximate solution to the differential equations is to divide the volume of a structure or system in to smaller (finite) elements such that infinite number of DOFs is converted to a finite value. The sequence of steps involved in solving the equation of motion is as follows [19]

- Conversion of a structure in to a system of finite elements which are interconnected at the nodes and defining the DOF at these nodes.

- Determination of element stiffness matrix, the element mass matrix, and the element force vector for each element in a mesh with reference to the DOF for the element. The force –displacement relation and inertia force- acceleration relation for each element can be written as

$$(\mathbf{f}_S)_e = \mathbf{k}_e \mathbf{u}_e \quad (2\text{-}23) \qquad (\mathbf{f}_I)_e = \mathbf{m}_e \ddot{\mathbf{u}}_e \quad (2\text{-}24)$$

where $\mathbf{k}_e$ is the element stiffness matrix, $\mathbf{m}_e$ is the element mass matrix, $\mathbf{u}_e$ and $\ddot{\mathbf{u}}_e$ are the displacement and acceleration vector for the element.

- Formation of transformation matrix (Boolean matrix contains zeros and ones) that connects the values of each element in to the global finite element assemblage. It simply locates the elements of $\mathbf{k}_e, \mathbf{m}_e$ and $\mathbf{u}_e$ at the proper places of the global matrices. For instance the elemental displacements $\mathbf{u}_e$ can be related to global matrix $\mathbf{u}$ through the following expression

$$\mathbf{u}_e = \mathbf{a}_e \mathbf{u} \quad (2\text{-}25)$$

- Assembling of element matrices to evaluate the global stiffness, mass matrices and applied force vector for the final assemblage

$$\mathbf{k} = A_{e=1}^{N} \mathbf{k}_e \quad (2\text{-}26) \qquad \mathbf{m} = A_{e=1}^{N} \mathbf{m}_e \quad (2\text{-}27)$$

$$\mathbf{p}(t) = A_{e=1}^{N} \mathbf{p}_e(t) \quad (2\text{-}28)$$

where A is an operator responsible for assembly process. According to the transformation matrix $\mathbf{a}_e$, the element mass matrix, element stiffness matrix and element force vector are placed in the respective global matrices and the arrangement is based on the number of an each element $e = 1$ to $\mathbf{N}e$, where $\mathbf{N}e$ is the number of elements.

- The final equation of motion with the global matrices is formulated as in the form of basic governing equation. This equation can be solved for $\mathbf{u}(t)$ using an appropriate iteration schemes which gives the response of system in term of nodal displacement values.

Apart from this sequence of steps, the values of element mass matrix $\mathbf{k}_e$, element stiffness matrix $\mathbf{m}_e$ and element force vector $\mathbf{p}_e(t)$ are determined by a function called element shape function or interpolation function.

2.4.2 Modal analysis

Generally, modal analysis is used to determine the vibrational characteristics of a structure. The vibrational characteristics such as natural frequencies and mode shapes of a structure are important in designing a structure subjected to a dynamic load. It can be considered as a starting point for a transient dynamic analysis. Also, the response of a structure can be evaluated when these modes are excited. The basic equation used in undamped modal analysis is the classical eigen value problem which is given as

$$\mathbf{k}\boldsymbol{\varphi}_i = \omega_n^{\,2} \mathbf{m}\boldsymbol{\varphi}_i \quad (2\text{-}297)$$

where φ_i is a mode shape vector (eigen vector) of mode i and ω_n is a natural frequency of mode *i.* As described in section 2.3, wave loads are highly non-linear and time varying and this necessitates the consideration of a dynamic response of offshore structures. If the period of a wave is close to a natural frequency of a structure and also if the applied load drives the mode shapes then it leads to the resonance and failure of a whole system. So it is an essential process to find out the natural frequencies and its mode shapes of a structure. Generally, the dynamic response of a structure is measured by a parameter called Dynamic Amplification Factor (DAF) which is defined as a ratio of dynamic response amplitude to the corresponding static response. The analysis setup and results of modal analysis are given in the later sections of the report.

2.5 System coupling

2.5.1 Work flow

In ANSYS Workbench, the FSI (one-way and two-way coupling) analysis can be performed by connecting the coupling participants to a component system called System Coupling. A participant system is a system which either feeds or receives data in a coupled analysis. Here, Fluent (participant 1) and ANSYS Mechanical (participant 2) are acting as coupling participants.

Figure 2-6 depicts the work flow of a FSI simulation using System Coupling with coupling participants [16]. Initially, system coupling collects information from the participants to synchronize the whole set up of simulation and then the information to be exchanged are given to the respective participant. The next step of the work process is organizing the sequence of exchange of information. The solution part of the chart varies for different ways of coupling. Finally, the convergence of coupling step is evaluated at end of the every coupling iteration.

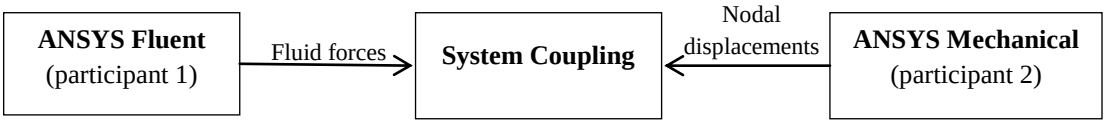

Figure 2-6 System Coupling - flow chart

In the case of one-way coupling, it follows the work instruction as mentioned in section 2.1.3. As it launches the first time step, Fluent iterates until convergence is attained and transfers the pre-requested information (fluid forces) to ANSYS Mechanical, so that this solver begins the iteration process for the same time step to get converged nodal displacements. Now, the coupling service (System Coupling) collects the convergence status from both the participants and launches next time step.

On the other hand, two-way coupling has a more intrinsic solving facility which follows the work sequence as described in section 2.1.4. As any time step (coupling step) is launched, Fluent acquires a converged solution according to its own criterion of the convergence and transfers the fluid forces to ANSYS Mechanical. Then the displacement value of a structural member is obtained with help of the solution provided by Fluent for the same time step. Now the difference exists compared to the one way coupling. The calculated solution of ANSYS Mechanical is given back to the

Fluent to determine a new set of fluid forces according to nodal displacements of previous time step. This is said to be a coupling iteration and continues until the convergence criterion of data transfer is reached.

2.5.2 Data transfer

Data transfer between the coupled participants is one of the critical parts of an FSI analysis. At the interface of the two mediums, the information has to be exchanged between two different meshes of different mediums. This is carried out by a systematic sequence and it includes some sub processes.

The first process of the data transfer is to match or pair the source and target mesh to generate weights. The source mesh feeds the data to the target mesh and this matching is done by two different mapping algorithms in System Coupling according to the nature of the data transferred.

The first algorithm is called the General Grid interface (GGI) which uses the method of dividing the element faces of both target and source sides into n (number of nodes on each side) integration points (IP). These three dimensional IP faces are converted into two dimensional quadrilaterals, which are made up of rows and columns of pixels. Pixels of both target and source sides are intersected to get overlapping areas called control surfaces. Finally, mapping weight contributions are determined for each control surface by the amount of pixel interactions, these interactions are accumulated to get the value of mapping weights for each node [16]. The mapping weights generated by this algorithm are conservative in nature, so it is used as a default algorithm in Workbench for transferring the quantities like forces, mass and momentum. The conservative nature of GGI algorithm is shown *Figure 2-7*.

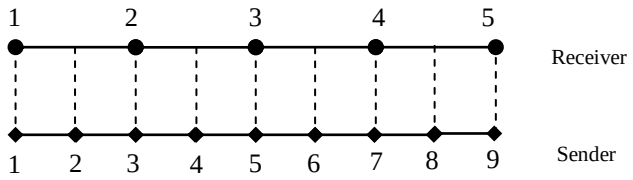

Figure 2-7 Conservative nature of GGI algorithm [16]

The next one is the `Smart Bucket algorithm' shown in *Figure 2-8*; in this algorithm, the process of computing the mapping weights starts by dividing the target mesh in to a grid of buckets (simple group of elements on a mesh). Then mapping weights are computed for each node on the source mesh which is already associated with the buckets of target mesh. Two cases of buckets can exist i.e. empty (no element inside it) and non-empty (contain elements) bucket. In the latter case, the source node is matched to one or more elements in the bucket of target mesh and this is executed by iso-parametric mapping. For the case of an empty bucket, the closest non-empty bucket is identified and the same procedure is followed using iso-parametric mapping [16]. Due to the profile preserving nature of the generated mapping weights, this is used as a default algorithm in Workbench for transferring the non-conserved quantities such as displacement, temperature and stress.

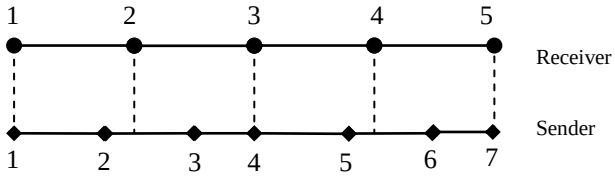

Figure 2-8 Profile preserving nature of Smart Bucket algorithm

It can be concluded that the fine mesh must be used on the sending side when conservative algorithm is used in order to send as much information as possible, on other hand for the profile preserving algorithm, the receiving side should have the refined mesh for the purpose of capturing sufficient information. Finally, interpolation algorithms are accountable for target node values with the help of source data and mapping weights generated by any one of the above algorithms.

3 Methodology

The purpose and explanation of the problem are given in section1.1 and 1.2 respectively. A brief introduction to the overall method is given in this section. Initially, geometric models of both fluid and solid domains are created with appropriate dimensions. ANSA is used as a preprocessor for creating the geometries models. The surface and volume mesh of fluid domain are formed using ANSA and the finite element mesh is created by ANSYS Meshing. The two computational meshes differ with parameters such as cell type, cell size and mesh resolution. The completed meshes are imported to the respective numerical solvers where the simulation setup of a model is implemented. The simulation setup includes essential steps such as assigning the material properties, boundary conditions and numerical schemes for the two different models. At the end of the simulation setup, the fluid model consists of two mediums (water and air) where the cylindrical member is placed near to a free surface of the water such that the wave passes the cylinder within desired time period, whereas the structural model is a simple cylindrical member with its ends fixed in position. Finally, the two solvers are coupled in Workbench using System Coupling to exchange the data according to the type of coupling. A simple sketch of a wave approaching the cylinder is shown in *Figure 3-1*.

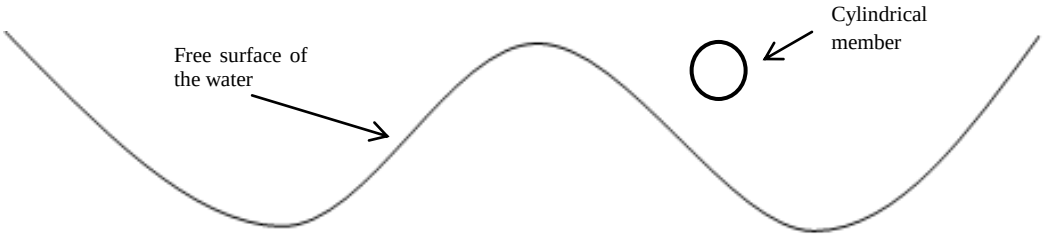

Figure 3-1 Wave approaching a cylinder

3.1 Geometry

The fluid domain is made as a square prism in which the cylindrical member is placed inside. *Figure 3-2* shows the entire fluid domain with dimensions and *Figure 3-3* shows a closer view of the structural member fixed at the symmetrical walls of the fluid domain. The structural member is placed at a height of 6m above the sea water of depth 49m. This member is surrounded by a larger cylinder and boxes of two different sizes and these are created in order to make a refined mesh around the structural member. The vertical and horizontal distance of the domain is taken as 180m to avoid the velocity gradients at the upper boundary and reflections from the outlet boundary respectively.

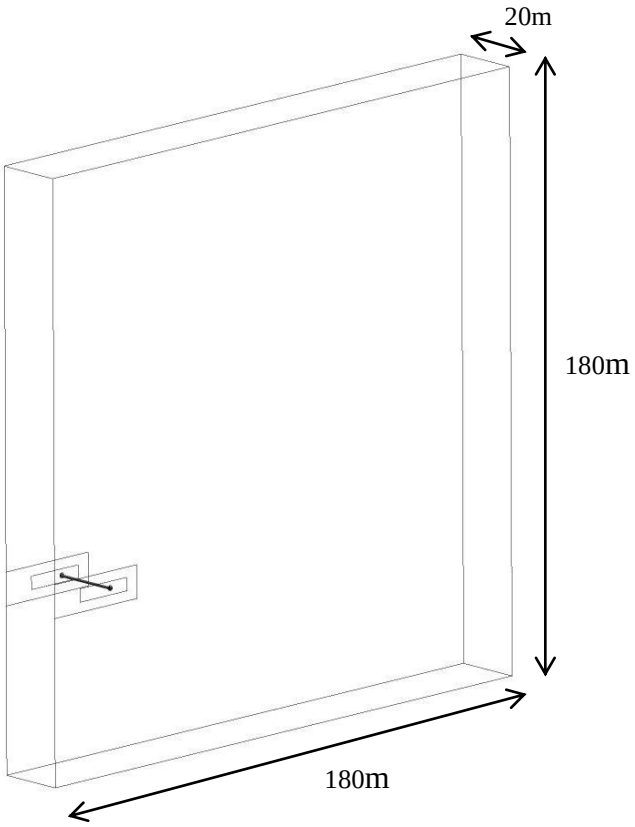

Figure 3-2 Geometry of a fluid domain

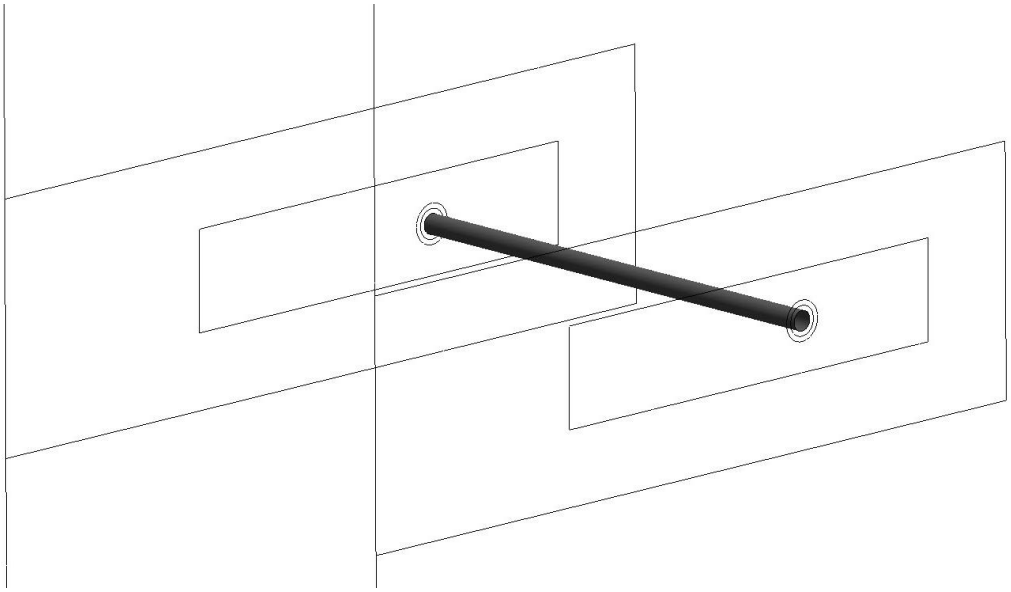

Figure 3-3 Closer view of cylinder fixed at the symmetric walls of the fluid domain

The geometry of the structural member for the purpose of transient structural analysis is shown in *Figure 3-4*. The position of the structural member in the CSM model is identical to the position of the cylindrical wall in the CFD model; otherwise it would lead to errors while transferring data between two solvers.

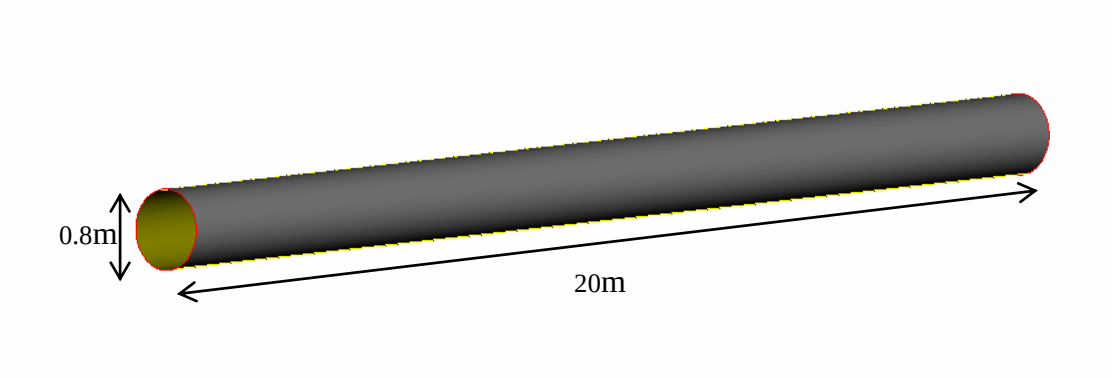

Figure 3-4 Structural member

3.2 Computational mesh

In the case of the CFD mesh, the surface mesh is first created using triangular elements, which is then used to create a volume mesh. The volume mesh is made up of tetrahedral cells, belonging to the category of unstructured mesh. Unlike the structured mesh, the cells of unstructured mesh cannot be identified using i, j, k index. The reason for not using hexahedral cells is that it is not compatible with the use of dynamic mesh in the current version of ANSYS Fluent. The mesh of the entire computational fluid domain is shown below.

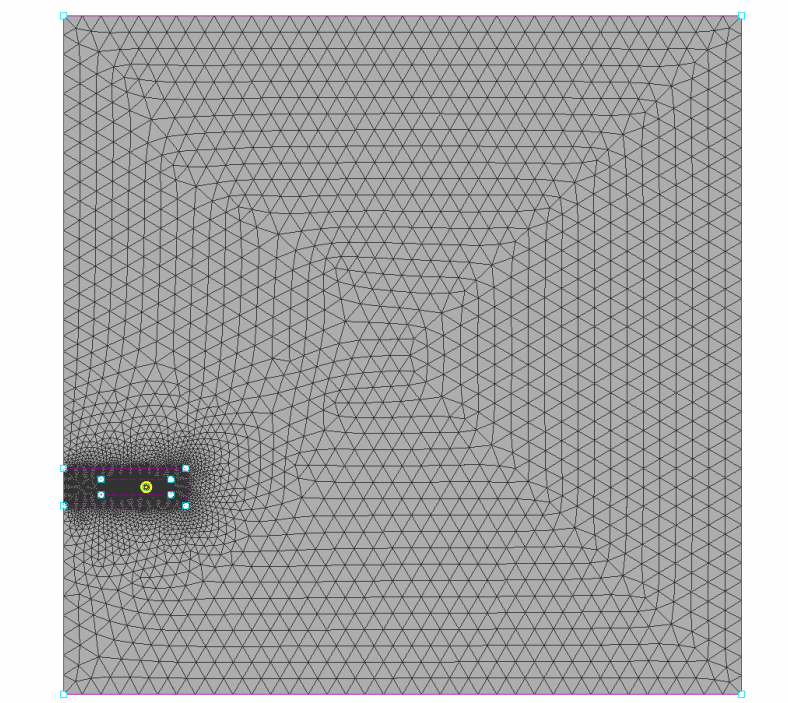

Figure 3-5 Computational mesh of the fluid domain.

The volume mesh of the fluid domain also includes the prism layers (shown in *Figure 3-6*) around the cylinder's wall to resolve the boundary layer more efficiently than what can be achieved with tetrahedral cells. Prism layers are made up of cells which

are almost perpendicular to the surface of the cylinder. This is used for better resolution of solution normal to the surface of the cylinder. The spacing of prism layers is an important factor in order to get a good solution, apart from this, emphasis must be given to the parameters like initial height of the layer, number of layers and growth ratio of prism layers to capture the boundary layer effect in realistic manner.

Generally, boundary layers require a special treatment in a CFD model. In this treatment, y^+ value (non-dimensional distance from the wall to the first cell) is considered to be an important parameter. Wall functions of the turbulence model deal with the flow in the boundary layer and have some restrictions on the y^+ values at the wall. The usual range limit of y^+ value is considered as 15- (100-1000) [16]. In order to maintain the y^+ value in this range, an initial height of ~1.95mm is evaluated according to [25]. This indicates that the first prism layer must be placed in the same height of 1.95mm. Along with this, an x-y plot (velocity vs vertical distance) has been taken using Fluent (see Appendix 6B) to find the boundary layer thickness. The approximate boundary layer thickness appears as double the diameter of the structural member from the plot. So, a larger cylinder of diameter equal to 0.8m (shown in *Figure 3-6*) is created around the structural member such that, the most refined mesh is created between these two cylinders to resolve the boundary layer flow . Also, two boxes of different dimensions have been created above the larger cylinder for the purpose of tracking the free surface of the water and the flow around the structural member in a better way. Finally, a small calculation has been done to find out the spacing and number of prism layers according to the height of first tetrahedral cell. As per the calculation, twelve layers of prism with a growth ratio of 1.5 are determined.

In the interest of conducting a mesh convergence study, two meshes of different resolution have been created. This is one of the important steps in the CFD analysis to make sure that the solution of the problem is independent of mesh resolution. *Figure 3-6* and *Figure 3-7* show the fine and coarse mesh respectively.

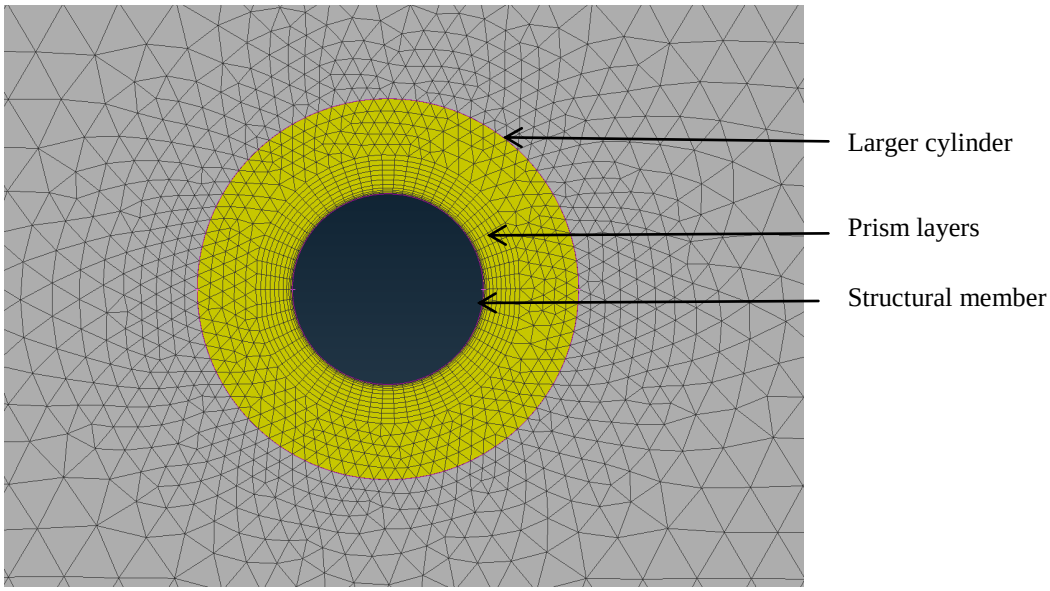

Figure 3-6 Refined mesh

The refined mesh contains around 4.65 million cells, whereas the coarse mesh contains 3.36 million cells.

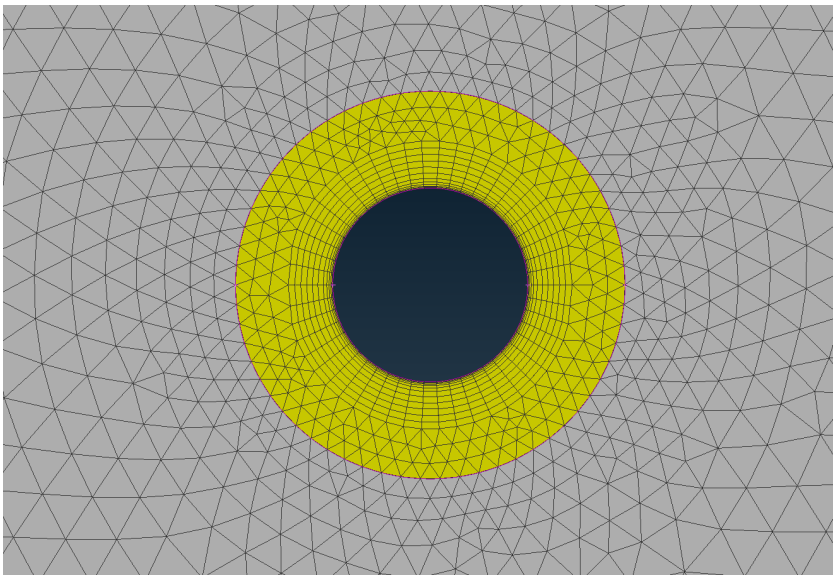

Figure 3-7 Coarse mesh

The computational mesh of the structural member is created with the help of ANSYS Meshing tool. *Figure 3-8* shows the mesh of structural member.

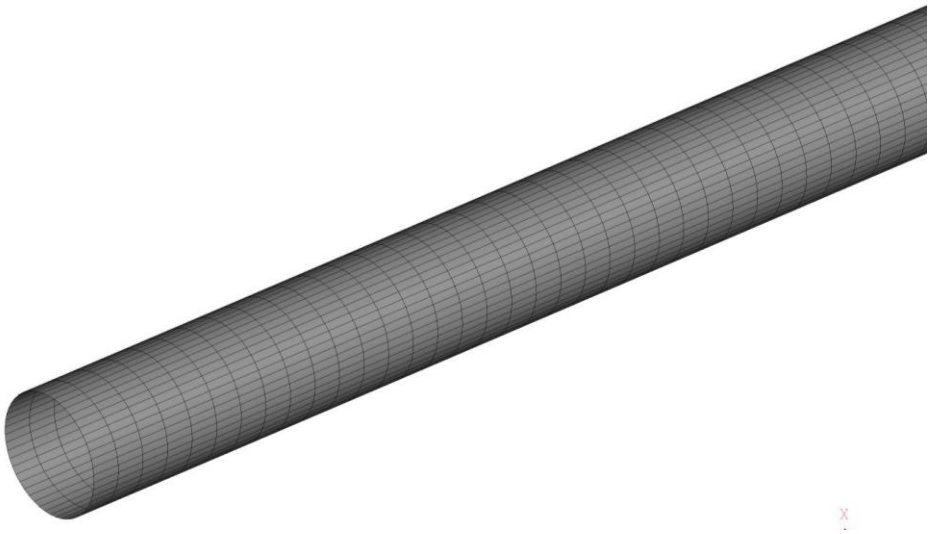

Figure 3-8 Structural mesh

The whole CSM finite element mesh consists of 5000 shell elements. The type of shell element used here is SHELL181. This is the standard and suitable element used by ANSYS Mechanical for analysing structures with thin to moderately thick shell structures. It is a four-node element with six degrees of freedom at each node. Six degrees of freedom include translations in the x, y and z directions and rotations about the x, y and z axes [16].

3.3 Different cases of simulation

As stated in section 1.3 , the FSI analysis has been conducted to evaluate the difference between two methods of coupling under various deformation patterns of the structural member subjected to wave loads. In order to achieve a large variation of deflections without re-meshing the model, different material properties have been considered for the work. These cases are formed by varying the thickness and Young's modulus of the material. Firstly, in order to get a rough estimate about the deflection of the structural member, an analytical method has been applied (see Appendix C). This calculation has been done for different cases varying the thickness and Young's modulus of the structural member. The following three cases have been finally selected to reach reasonable conclusions from the work.

Table 3-1 Three different cases of structural member

Cases	**Thickness (mm)**	**Young's modulus (GPa)**
Case 1	15	10
Case 2	20	200
Case 3	20	50

3.4 Simulation setup

The computational work of this project is divided in to two parts, the first part deals with the wave model and the other is with the structural model. Subsequently, the simulation setups of this work also follow the same partition which is explained in the below sections.

3.4.1 Material properties

The fluid model is comprised of two phases, gas (air) and liquid (water). The important properties of both air and water used in this simulation are shown in *Table 3-2*. The different cases for the structural member as shown in section 3.3 are listed with the material properties in

Table 3-3. The simulation setup for the three different cases is exactly the same with linear material properties.

Table 3-2 Material properties of air and water

Phases	**Density (kg/m^3)**	**Dynamic viscosity (kg/ms)**
Air	1.225	$1.789.10^{-5}$
Water	998.2	$1.003.10^{-3}$

Table 3-3 Material properties for different cases of the structural member

Cases	Thickness (mm)	Young's modulus (GPa)	Poisson's ratio	Density (kg/m^3)
Case 1	15	10	0.3	7850
Case 2	20	200	0.3	7850
Case 3	20	50	0.3	7850

3.4.2 Turbulence modeling setup

The theoretical explanation of turbulent flow and its modeling is given in section 2.2.5. *Table 3-4* shows the type of turbulence model and wall function used.

Table 3-4 Turbulence modeling setup

Turbulence model	Realizable k-ε model
Near wall treatment	Non-equilibrium wall function

3.4.3 Multiphase modeling setup

The wave model involves the free surface flow which is tracked by using a multiphase model called VOF. The description about the multiphase flow, VOF model and types of scheme for finding volume fraction are explained in section 2.2.6. *Table 3-5* shows the simulation setup details of multiphase modeling used in Fluent.

Table 3-5 Multiphase Modeling setup

Multiphase model	Scheme	Options
Volume of Fluid (VOF)	Explicit	Open channel flow Open channel wave BC

3.4.4 Boundary conditions

Table 3-6 lists the boundary conditions applied on the boundaries of the fluid model shown in *Figure 3-9*.

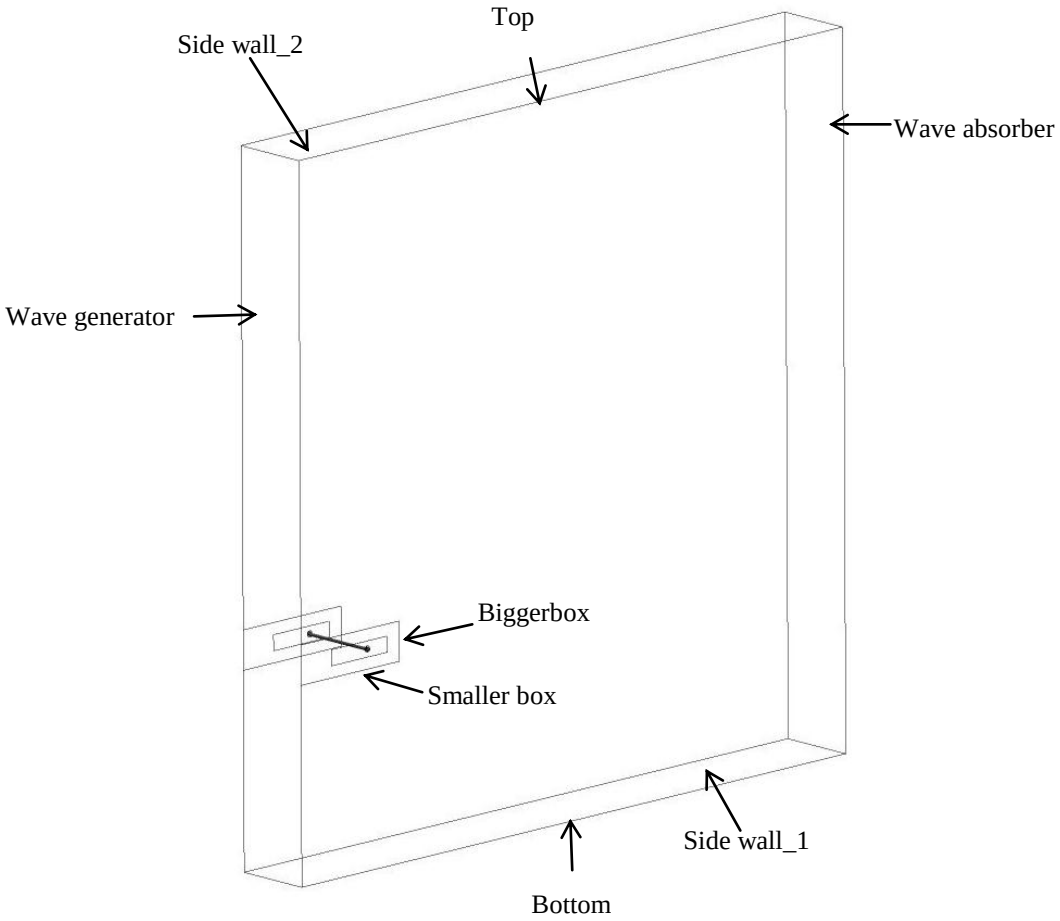

Figure 3-9 Boundary conditions of the fluid model

Table 3-6 Boundary conditions of a fluid model

Parts of the domain	**Type of boundary condition**
Wave generator	Velocity-inlet (open channel wave boundary condition)
Wave absorber	Pressure-outlet (open channel flow boundary condition)
Top	Wall (zero shear)
Bottom	Wall (zero shear)
Side wall_1	Symmetry
Side wall_2	Symmetry
Cylinder	Wall (no slip)
Bigger cylinder	Interior
Smaller box	Interior
Bigger box	Interior

Here, the open channel wave and open channel flow are the special type of boundary conditions used for wave modeling in Fluent. Open channel wave boundary condition is chosen to simulate the propagation of waves. This is executed by selecting the appropriate wave theories according to the wave properties. Open channel flow condition is implemented in modeling the open channel flows such as rivers, dams and ocean waves. These flows involve the free surface between two phases which is solved using VOF formulation [16]. *Table 3-7* shows the specification of open channel wave boundary condition. Open channel flow condition is applied with similar specifications as the former one. The specifications of open channel wave boundary condition are selected with the help of chart (*Figure 3-10*) provided by Le Mahaute. The free surface height of the wave for the chosen wave characteristic parameters is shown in *Figure 3-11*.

Table 3-7Specification of Open channel wave boundary condition

Open channel wave boundary condition			
Multiphase flow setup		**Turbulent flow setup**	
Wave theory	5^{th} order Stokes wave theory	Turbulence specification method	Intensity and length scale
Wave amplitude	5 m		
Wave length	90 m	Intensity	1 %
Free surface level	49 m	Length scale	0.1 m

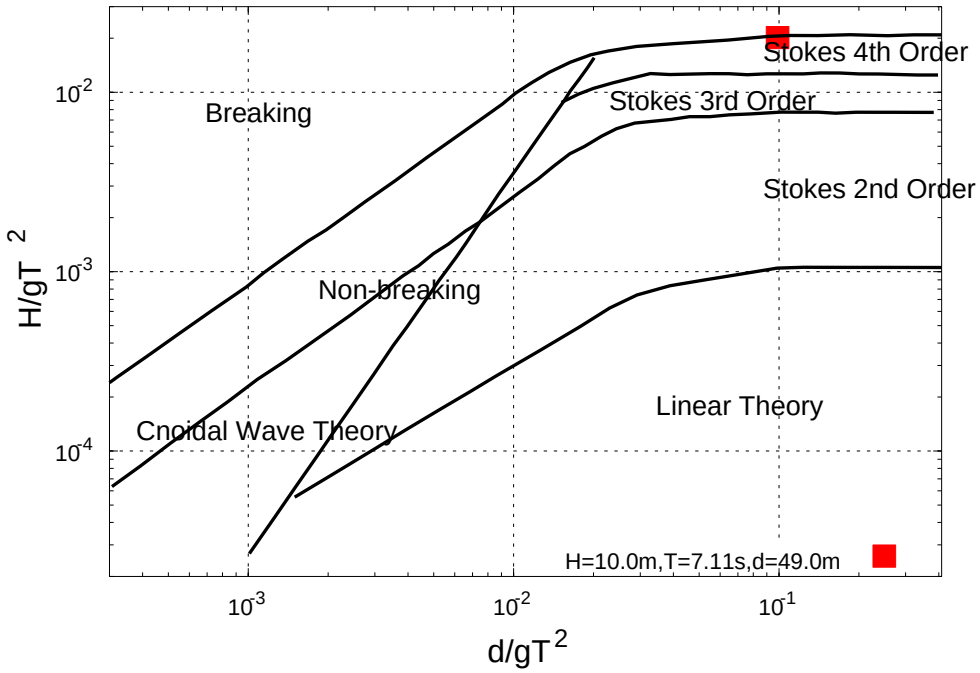

Figure 3-10 Validity Range of different wave theories [24]

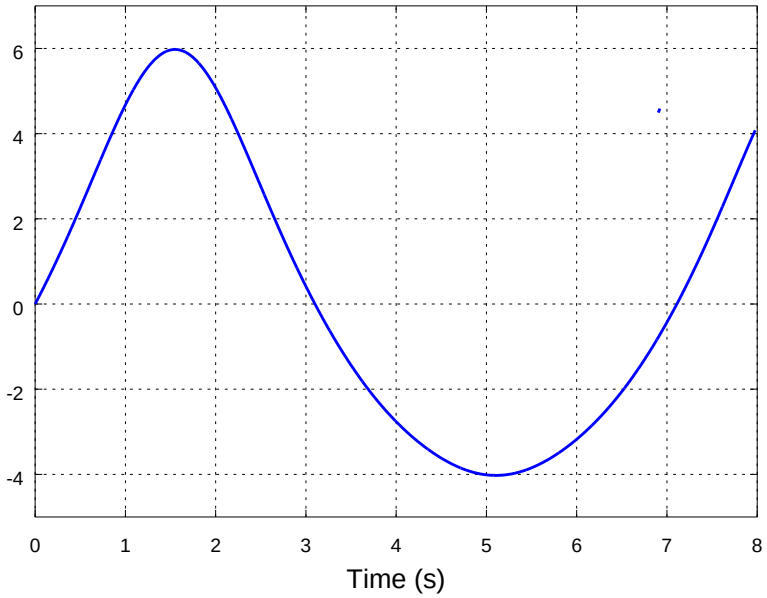

Figure 3-11 Free surface height of the wave used in the fluid model

Apart from this, in the case of two- way coupling, dynamic mesh settings have to be added in order to get a mesh deformation. The important step of this part is to assign dynamic mesh zones among the boundaries of a fluid model. Here, all the symmetric boundaries are assigned to the *deforming* type of dynamic mesh zones, whereas the cylinder is allotted to the *System Coupling* type.

3.4.5 Solver setup

The below table lists the type of temporal and spatial discretization schemes used in Fluent. The number of time steps used is 2000 with step size of 0.001.

Table 3-8 Discretization scheme used in Fluent

Temporal discretization	First order implicit
Pressure-velocity coupling	SIMPLE
Spatial discretization	
Pressure	Body force weighted
Momentum	Second order upwind
Volume fraction	Compressive
Turbulent kinetic energy (k)	First order upwind
Turbulent dissipation rate (ε)	First order upwind

3.4.6 ANSYS Mechanical setup

The simulation setup of ANSYS Mechanical is simple compared to Fluent. The setup work consists of defining the boundary conditions, loads and analysis settings.

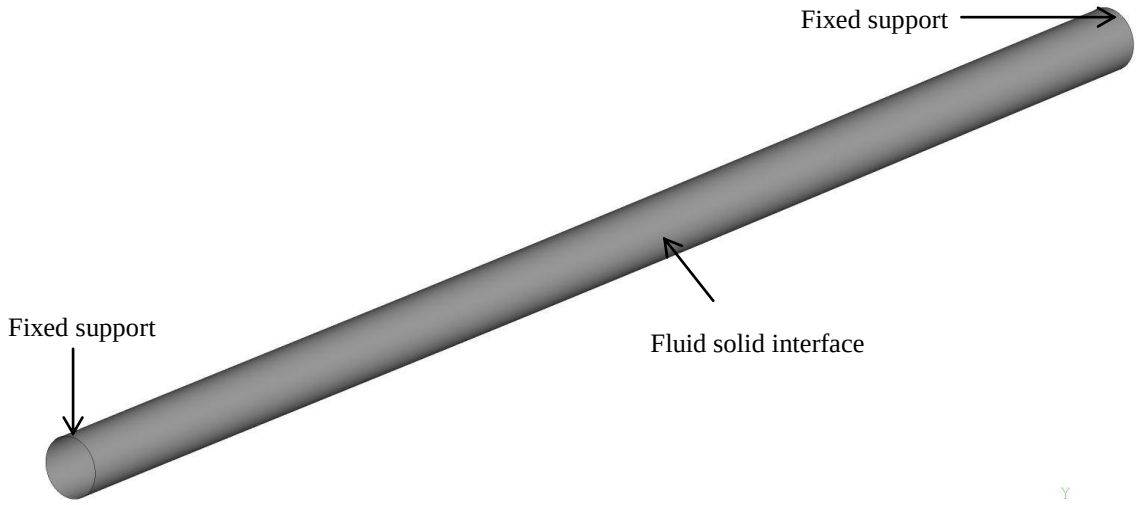

Figure 3-12 Simulation setup of a structural member

Figure 3-12 shows the overall simulation setup of the structural member. The end edges of the cylinder are fixed and the calculated fluid forces are applied on the surface of the cylinder which is described as a fluid solid interface. Apart from this, it follows the same transient setups like time step size and end time as in Fluent.

As mentioned in section 2.4.2, modal analysis has been performed to determine the natural frequencies and its associated mode shapes using ANSYS Mechanical. The analysis has been conducted for all three cases shown in 4.1. Firstly, geometry of the model is imported into the modal setup of Workbench. The Young's modulus of the structure and thickness are chosen according to the different case. Meshing procedure of the model is similar to the one followed for the structural analysis as in section 3.2. Then, end edges of the cylinder are prescribed with the fixed support boundary condition. Lastly, the number of mode shapes to find can be selected from analysis settings.

3.4.7 System Coupling setup

System coupling is a coupling tool used in Workbench to integrate different domain solvers in multi-physics simulations. The working principle and procedure of System Coupling is shown in section 2.5. Here, the simulation setups of System coupling and the FSI analysis of this project work are explained.

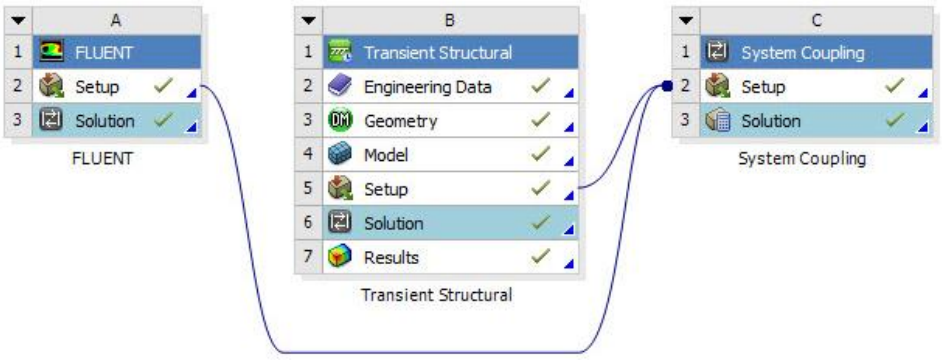

Figure 3-13 FSI analysis setup using System Coupling

Figure 3-13 depicts the FSI analysis setup of this project work using System coupling with Fluent and ANSYS mechanical as numerical solvers. Initially, the simulation setups of both solvers in the preceding sections are executed, and then the setup component of the solvers is integrated into the setup component of System Coupling as shown. This makes the System Coupling to synchronize the numerical conditions of both solvers and to identify the fluid structure interface.

The next step is to assign the simulation setups in System coupling. This consists of three main steps.

- Analysis Settings: This setting includes time step size, end time and maximum & minimum number of coupling iteration for each time step. Generally, other than the coupling iteration for each time step, the required information is automatically fed in to System Coupling once the solvers are coupled.

- Data transfer: This is the most vital part of the coupling device which includes and manages the data transfer sequence between two numerical solvers. This data transfer process varies with the type of coupling. *Figure 3-14* shows the data transfer for one-way and two-way coupling analyses. One-way coupling analysis is carried out with single-way data transfer from Fluent to ANSYS Mechanical which transfers the forces, whereas two-way coupling has data transfer in both direction i.e. first one from Fluent to ANSYS Mechanical (forces) and the second one is from ANSYS Mechanical to Fluent (nodal displacements).

- Simulation sequence: The working sequence of the numerical solvers should be given here as an input.

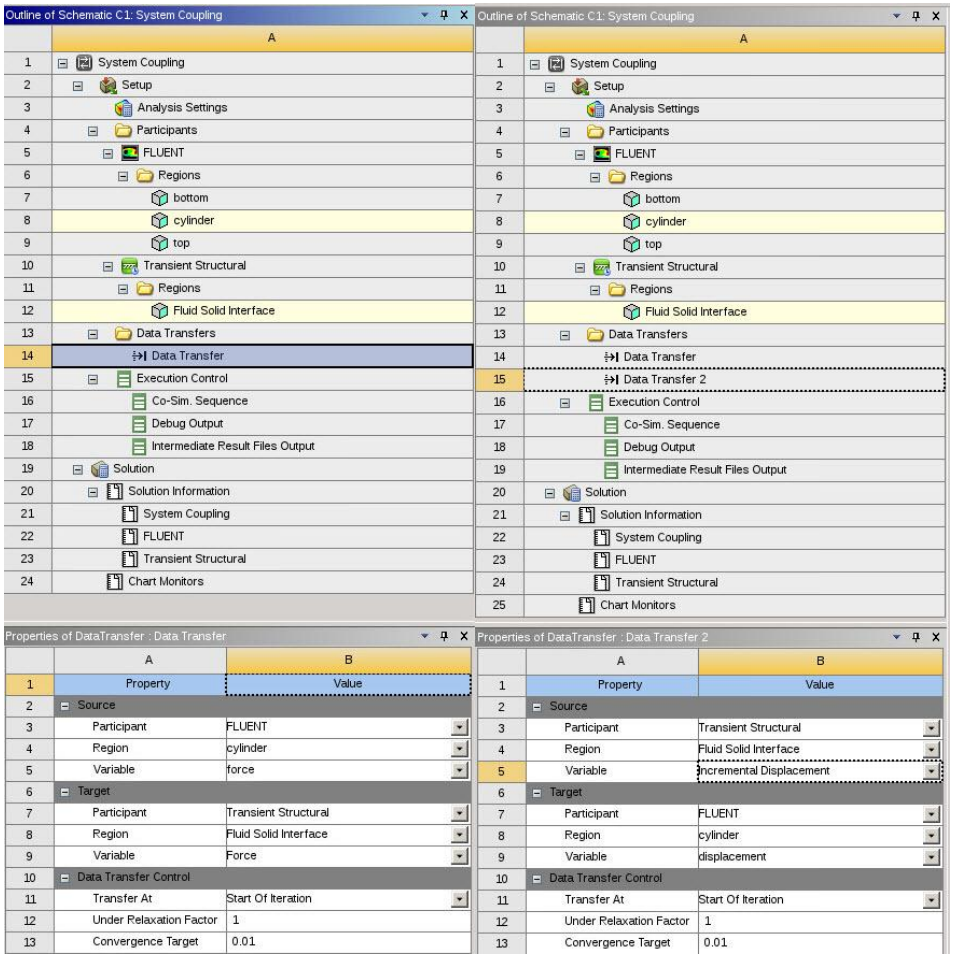

Figure 3-14 One-way coupling setup (left) Two-way coupling setup (right)

4 Results

4.1 Modal analysis

The results of modal analyses of three different cases are shown in *Figure 4-1*, *Figure 4-2* and *Figure 4-3* respectively. The result includes the first six mode shapes with its respective natural frequency values. The mode shapes (first, second, third and fourth) are similar in all three cases but with different frequency values. The first and second modes represent bending in x and y directions respectively. The third and fourth mode shapes show the S-shape in x and y directions respectively. Finally fifth and sixth modes are representing *Ovalisation* in two directions for case 1 whereas other type of S-shape is reflected in other two cases.

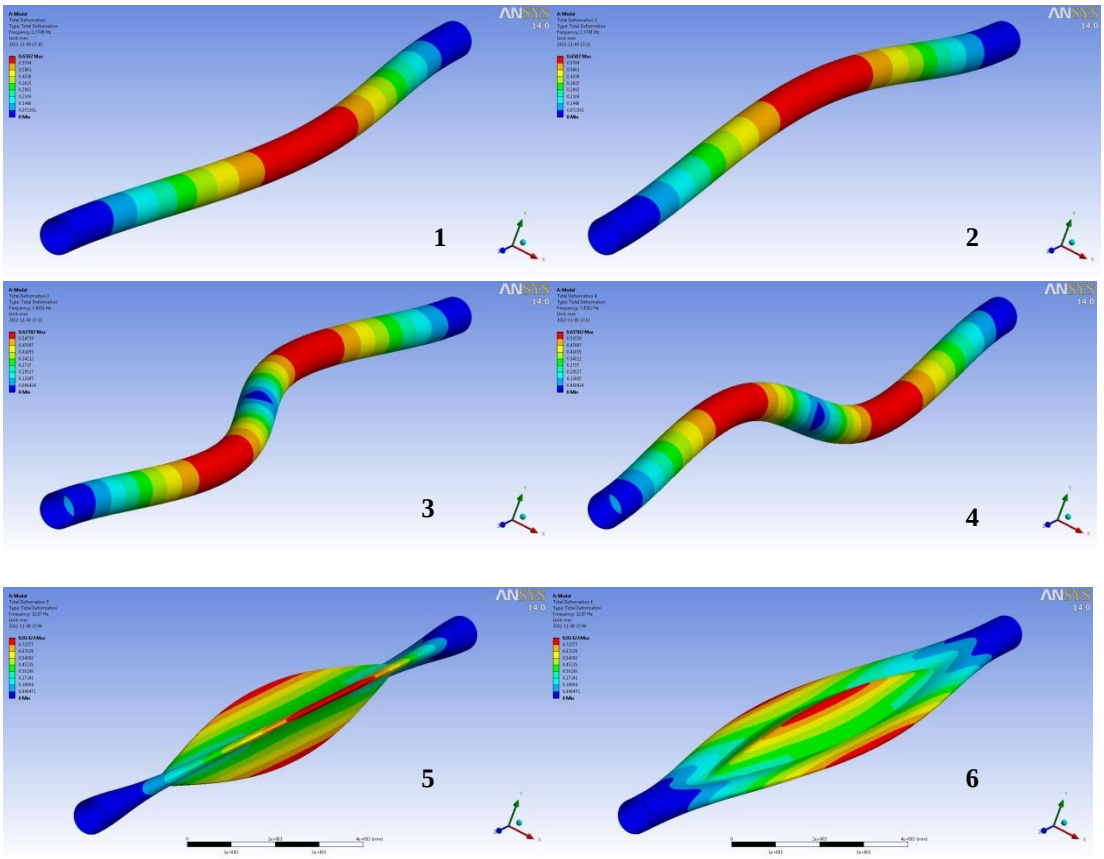

Figure 4-1 Six different mode shapes of case 1

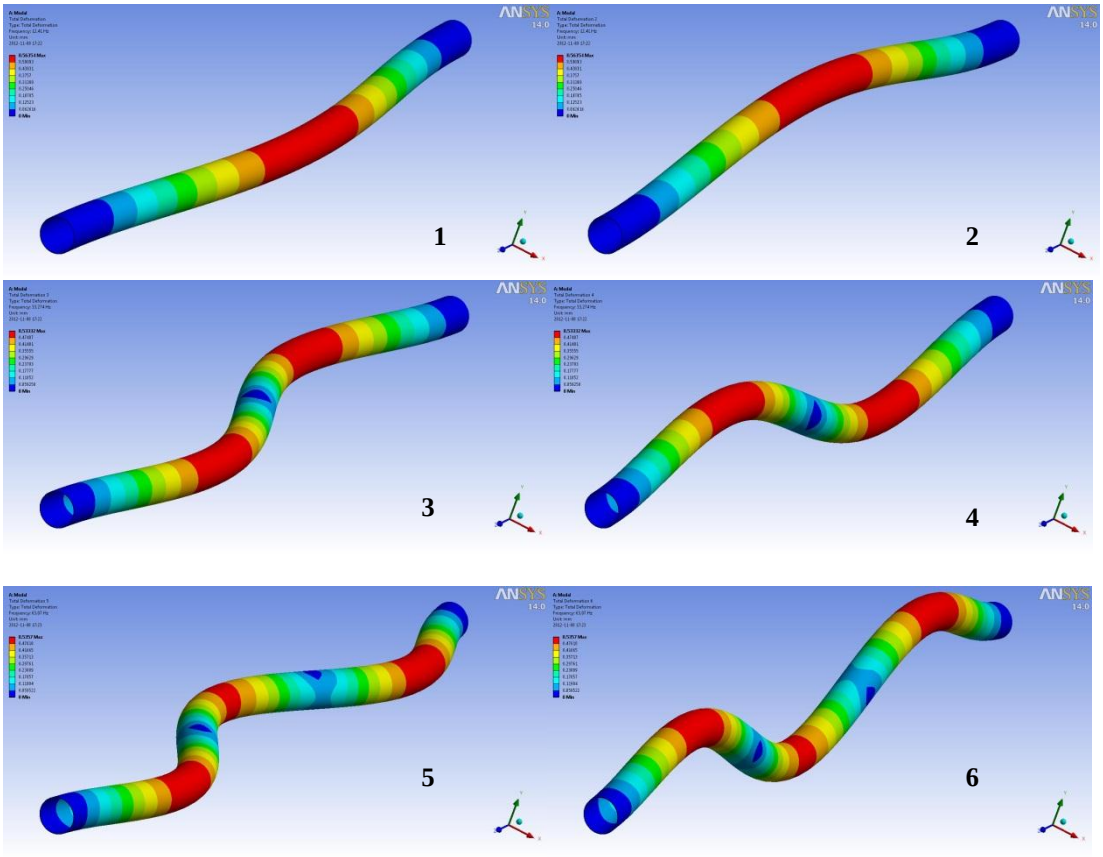

Figure 4-2 Six different mode shapes of case 2

Table 4-1 List of natural frequencies for three different cases

	Natural frequencies (ω_n) Hz		
Mode shapes	**Case 1**	**Case 2**	**Case 3**
1	2.77	12.41	6.20
2	2.77	12.41	6.20
3	7.43	33.27	16.63
4	7.43	33.27	16.63
5	13.87	63.07	31.53
6	13.87	63.07	31.53

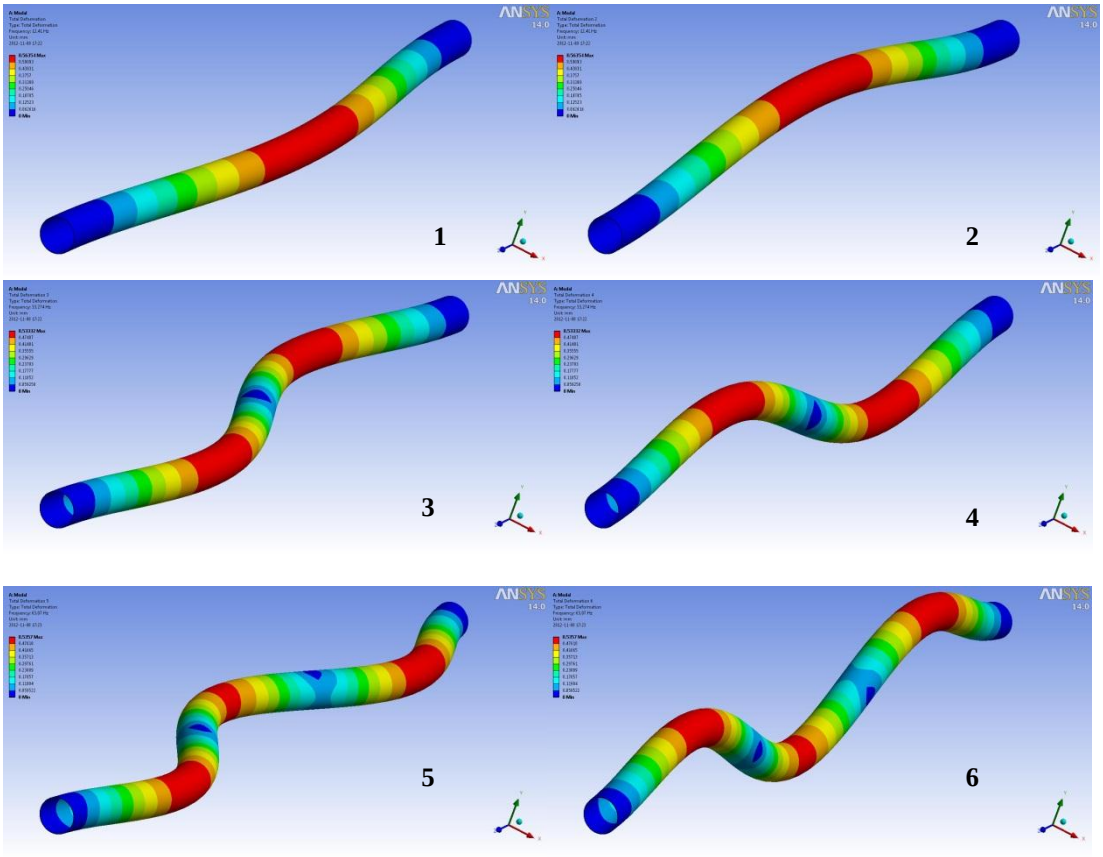

Figure 4-3 Six different mode shapes of case 3

4.2 Mesh convergence study

Two meshes with different resolution as shown in *Figure 3-6* and *Figure 3-7* have been created in order to perform a mesh convergence study. *Figure 4-4* shows the comparison of horizontal forces with two different meshes and *Figure 4-5* shows the comparison of vertical forces. In order to compare the meshes, slamming force of both cases are considered and a difference of 6% is observed between the peak values. So, it can be concluded from the comparison that the solution (force) is reasonably independent of the mesh resolution.

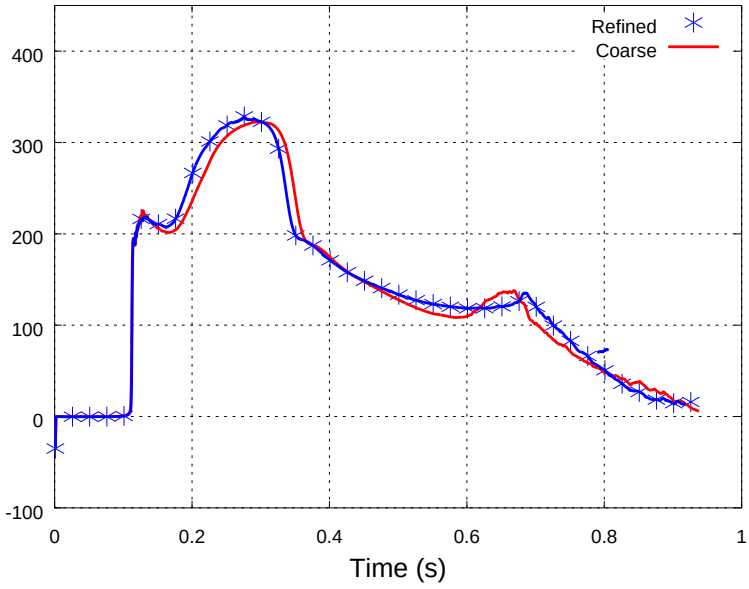

Figure 4-4 Comparison of horizontal forces for mesh convergence study

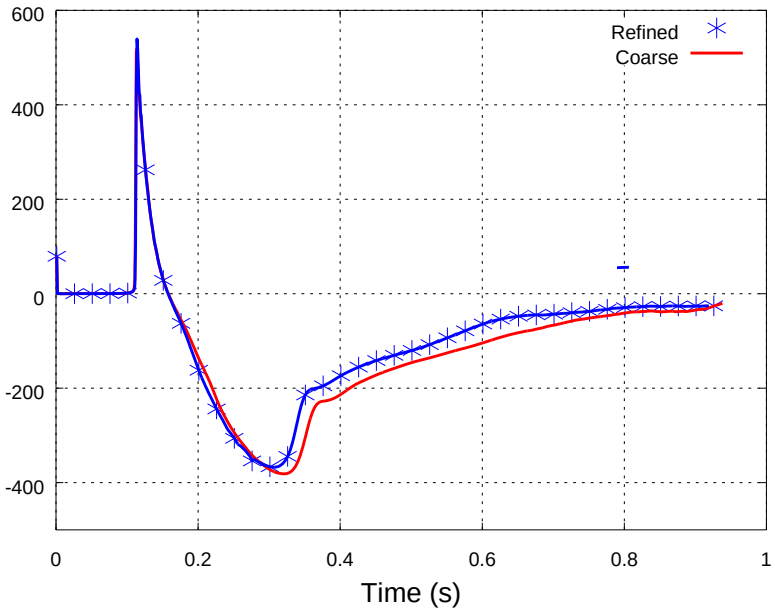

Figure 4-5 Comparison of vertical forces for mesh convergence study

4.3 Case1 (one-way)

Figure 4-6 shows the time history of CFD horizontal force (wave loads) and the reaction force (dynamic response) of the structural member for the one-way coupling simulation of case1. At the time of 0.112s approximately, free surface of the water touches the bottom side of the cylinder which gradually tends the CFD force to increase. The maximum horizontal force is attained by the time of around 0.330s. This is because, at this moment, the stagnation point of the flow is located at the front side of the member which leads to a high pressure difference in horizontal direction. Also, at the same time, flow starts to separate from the upper side of the structure. Then the

water flow tries to surround the structural member from both (upper and lower) ways which results in the gradual decrease of magnitude of the force. The dynamic response of the structure in both horizontal and vertical directions is extracted using ANSYS Mechanical. In this case, the forcing frequency (ω) is situated in the range of natural frequency (ω_n) of the structure which leads to the dynamic amplification of forces with DAF value of around 1.71. After this, the magnitude of reaction force is reduced a little and maintains the same trend of oscillation. This repetition is due to the absence of damping.

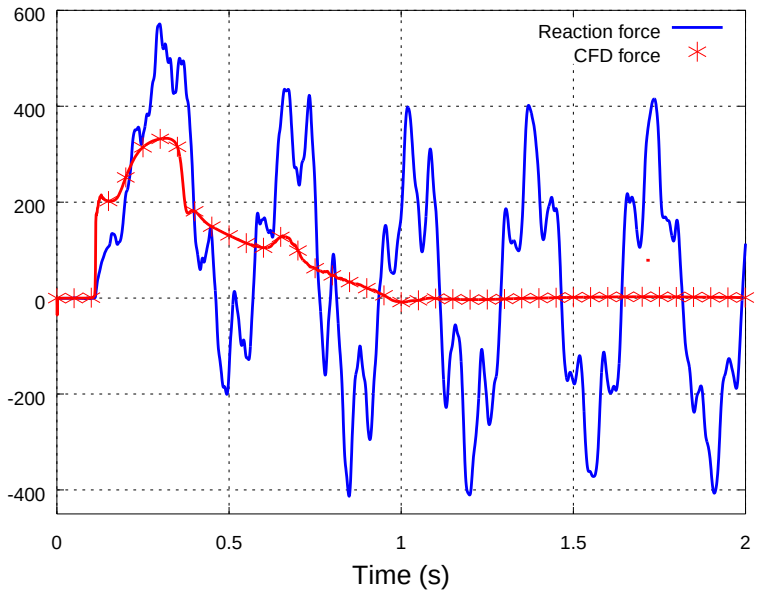

Figure 4-6 Horizontal (CFD & Reaction) forces of case1 (one-way) coupling simulation

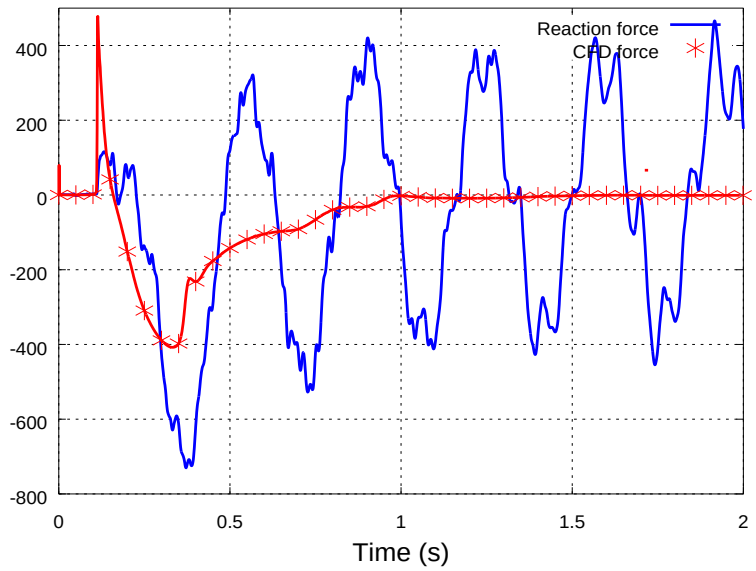

Figure 4-7 Vertical (CFD & Reaction) forces of case1 (one-way) coupling simulation

The time history of vertical CFD force acting on the cylinder and its corresponding response is shown in *Figure 4-7*. The peak vertical force (slamming force) is attained at the time of around 0.115s with the magnitude of 480kN approximately. The magnitude of the CFD force starts to decline in a steady way after it achieves the peak value. This is because as top of the wave starts to approach the structure with the high horizontal water particle velocities, a low pressure region is created at the bottom side of the cylinder. This leads to the development of negative vertical force and this reaches the minimum value at the same time as when the horizontal force reaches its maximum magnitude. The vertical force starts to recover after this point because the water starts to pass over the structure. As the dynamic response is concerned, the frequency of slamming force is very high compared to the natural frequency of the structure ($\omega >> \omega_n$). This results in the lack of amplification of reaction force for the peak vertical force. On the other hand, the reaction force is much amplified to the peak of negative vertical force with DAF value of 1.8 approximately, because the forcing frequency in the negative direction is in the range of natural frequency of the structural member.

Figure 4-8 shows the horizontal and vertical deformation of the structural member. This is taken with respect to a single point located at the center of the structure using CFD Post. It is very clear to notice that the deformation patterns are similar to the reaction forces. The major impact is observed in both directions when the reaction force is amplified and it maintains the consistent trend later due to the absence of damping.

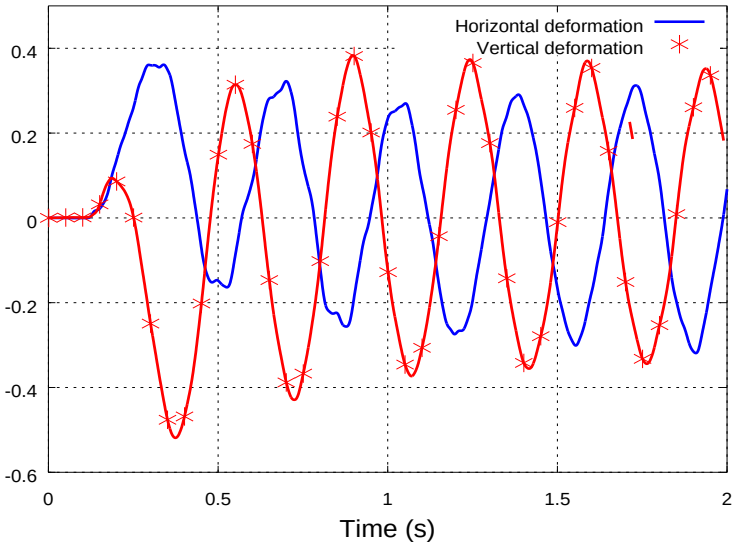

Figure 4-8 Horizontal and vertical deformations of the structural member - case1 (one-way).

4.4 Case1 (two-way)

Figure 4-9 shows the time history of CFD horizontal force (wave loads) and the reaction force (dynamic response) of the structural member for the two-way coupling simulation of case1. Significant differences can be seen between the curves of one-way and two-way coupling simulations. The main occurrences of CFD forces are

almost in the same time as the one-way coupling shown in *Figure 4-6*. However, the major difference is noticed in terms of the dynamic response of the structure.

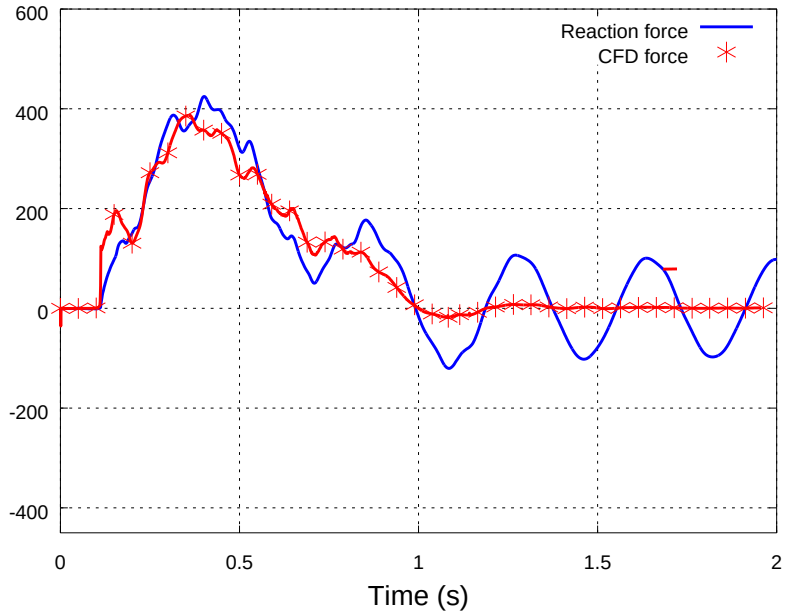

Figure 4-9 Horizontal (CFD & Reaction) forces of case1 (two-way) coupling simulation

The amplification of the reaction force is much smaller here because the difference in the behaviour of loading on the structural member. The magnitude of the reaction force subsides in the later stage because of hydrodynamic damping. Finally, the oscillation in the CFD force curve indicates that the fifth and sixth (ovalisation) mode shapes of this case have been activated as shown in *Figure 4-1*.

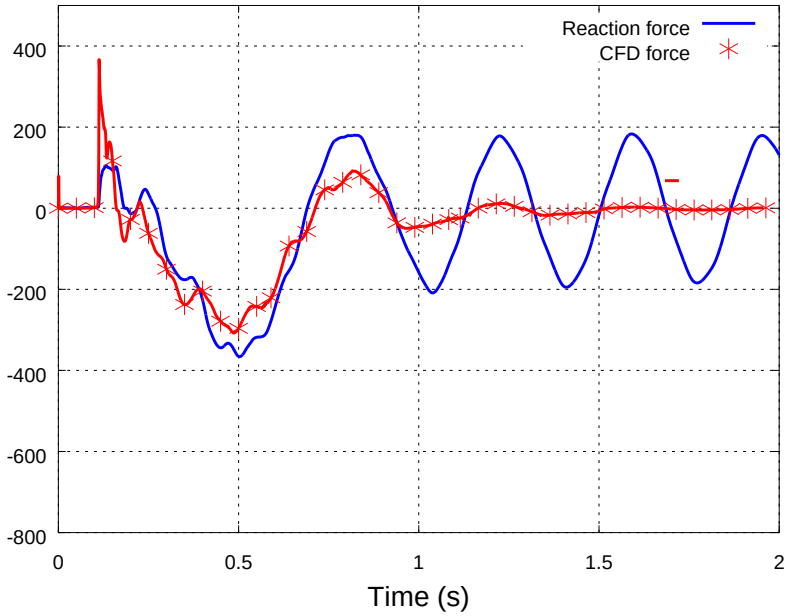

Figure 4-10Vertical (CFD & Reaction) forces of case1 (two-way) coupling simulation

The time history of vertical force acting on the cylinder and its corresponding response is shown in *Figure 4-10*. The peak value of the vertical force is achieved at the time of around 0.115 similar to one-way coupling, but the magnitude of the force is approximately 370kN, which is much lower than the previous one. This is because the structure is not as rigid as compared one-way coupling and made the force less intense. Also, as observed in horizontal force curve, the dynamic amplification is less due to the type of loading followed in the two-way coupling simulation. Since water acts as a dampener, the amplification of reaction force is less in the later stage.

Figure 4-11 shows the deformation in both directions. The displacement of the structural member is less compared to the case of one-way coupling, particularly the vertical displacement due to impact load. The displacement curves of one-way and two-way coupling have the same frequency which matches with the natural frequency of the structural member which could be observed from Power Spectral Density (PSD) plots shown in Appendix E.

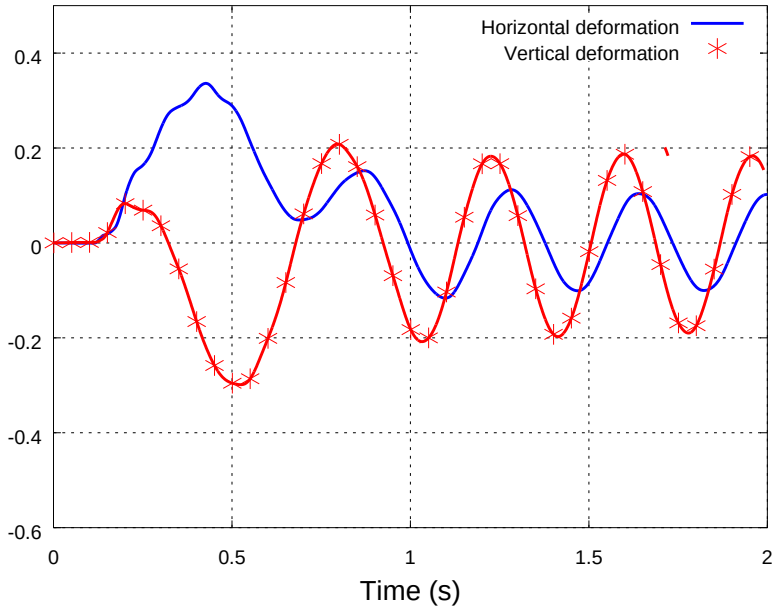

Figure 4-11 Horizontal and vertical deformation of the structural member- case1 (two-way).

4.5 Case2 (one-way)

Figure 4-12 shows the time history of CFD horizontal force (wave loads) and the reaction force (dynamic response) of the structural member for the one-way coupling simulation of case 2 (structural steel). The behaviour of CFD force curve is exactly the same in all three cases of one-way simulation as described in section 4.3, but the dynamic amplification is different for all cases. The reaction forces are amplified as the forcing frequency (ω) is situated in the range of natural frequency (ω_n) of the structure. Particularly, the first peak of CFD force with high frequency is the reason for the amplification of reaction forces, an approximate DAF value of 1.5 is observed. Later, the reaction forces maintain the same trend with the frequency of 12.5Hz which

matches with the natural frequency of the structure as shown in *Table 4-1*. The PSD plots of case 2 are shown in Appendix E.

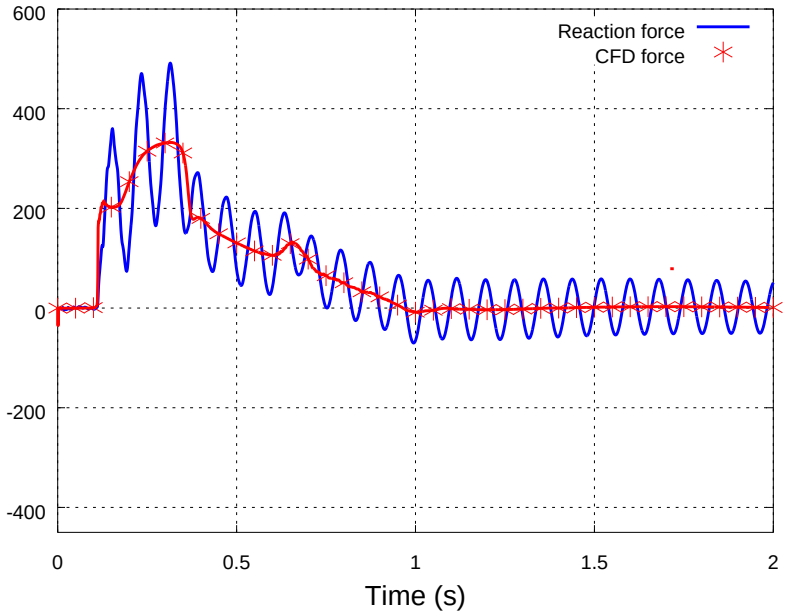

Figure 4-12Horizontal (CFD & Reaction) forces of case2 (one-way) coupling simulation

The time history of vertical force acting on the cylinder and its corresponding response is shown in *Figure 4-13*. The interesting outcome is that the reaction force is amplified to a good extent compared to case 1. This is because the frequency of the slamming force is in the range of fundamental frequency of the structure. The reaction force is amplified for the peak negative vertical force with DAF value of 1.68.

Figure 4-14 shows the horizontal and vertical deformation of the structural member. The displacement of this case is much smaller than the other cases. This is mainly due to the high stiffness of the material and later it sustains the same deformation pattern due to the absence of damping.

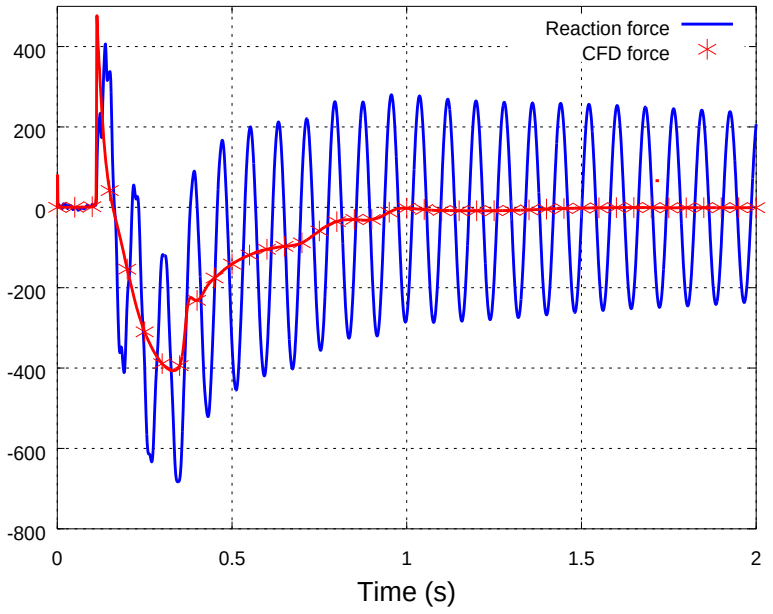

Figure 4-13 Vertical (CFD & Reaction) forces of case2 (one-way) coupling simulation

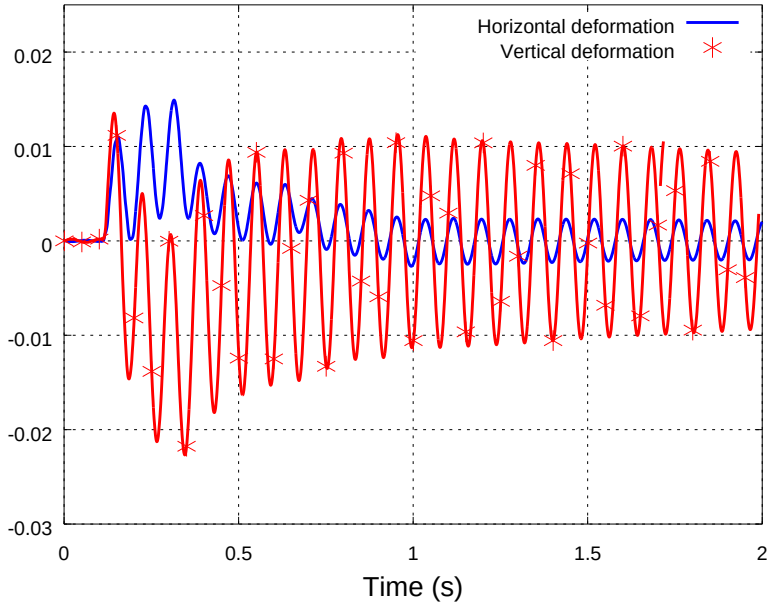

Figure 4-14 Horizontal and vertical deformation of the structural member- case2 (one-way)

4.6 Case2 (two-way)

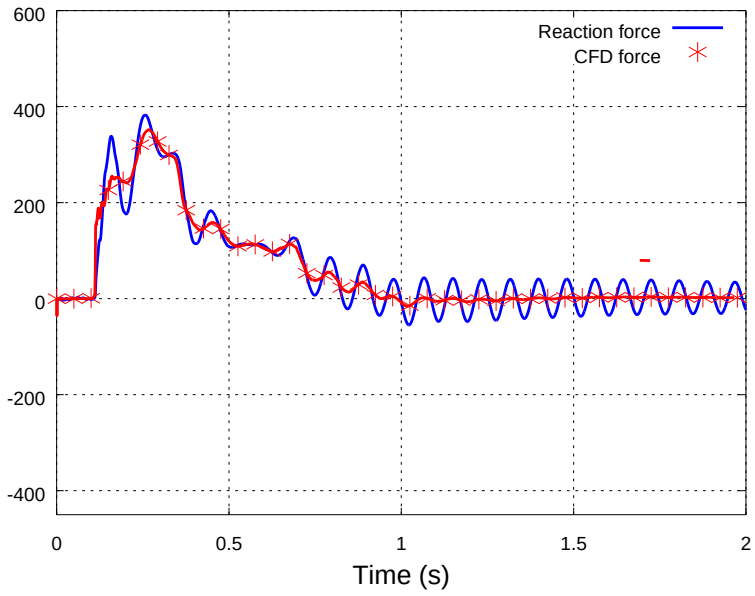

Figure 4-15 Horizontal (CFD & Reaction) forces of case2 (two-way) coupling simulation

Figure 4-15 shows the time history of CFD horizontal force (wave loads) and the reaction force (dynamic response) of the structural member for the two-way coupling simulation of case2. Differences can be seen between the both ways of coupling. The peak value of CFD force has almost same magnitude as one-way coupling method. The dynamic amplification is not as much as observed in one-way simulation because loads act differently and also due to the presence fluid damping.

The time history of vertical force acting on the cylinder and its corresponding response is shown in *Figure 4-16*. The peak value of the vertical force is reached at the time similar to one-way coupling and the magnitude of both cases has a smaller difference which implies the high stiffness and rigidity of the structure compared to case 1. Also, as noticed in horizontal forces, the dynamic amplification is less due to the behaviour of loads. Since water acts as a dampener, the amplification of reaction force is less in the later stage.

Figure 4-17 shows the deformation in both directions. The structural member is subjected to the slamming force and deforms in vertical direction almost to the same extent as the one-way simulation. Later it subsides because of the stiffness of the material and also for the type of load imposed in the two-way coupling method. The displacement curves of one-way and two-way coupling have same frequency which matches with the natural frequency of the structural member.

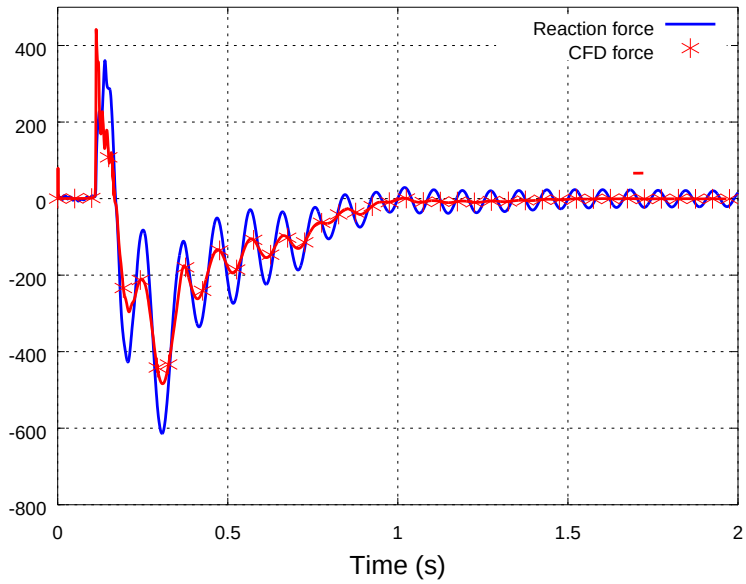

Figure 4-16 Vertical (CFD & Reaction) forces of case2 (two-way) coupling simulation

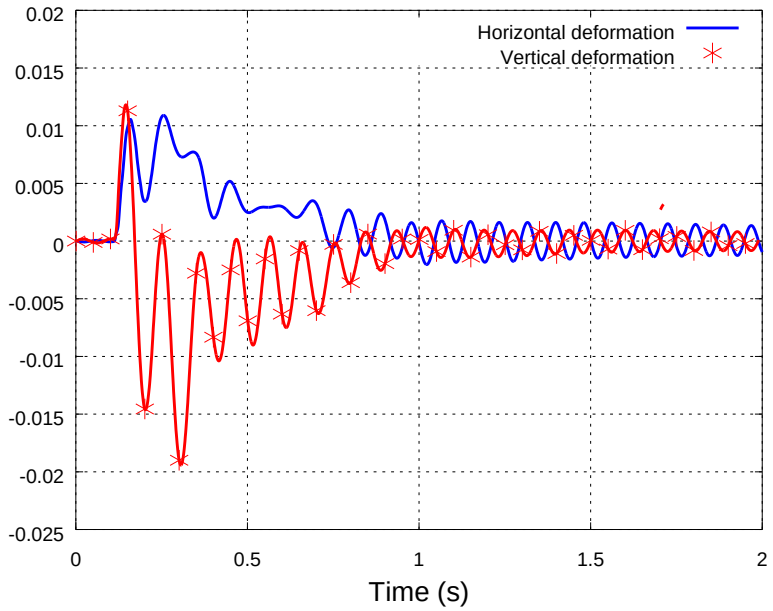

Figure 4-17Horizontal and vertical deformation of the structural member- case2 (two-way)

4.7 Case3 (one-way)

Figure 4-18 shows the time history of CFD horizontal force (wave loads) and the reaction force (dynamic response) of the structural member for the one-way coupling simulation of case 3. This case has the intermediate values of thickness and Young's modulus as compared with other two cases as given in *Table 3-1*. The CFD force curves are exactly similar in one-way simulations of all three cases, but the dynamic response of the structure varies.

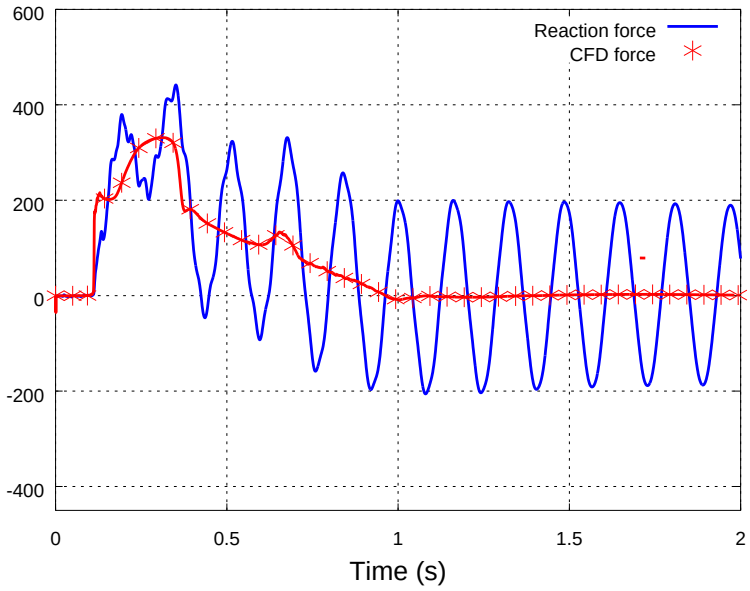

Figure 4-18Horizontal (CFD & Reaction) forces of case3 (one-way) coupling simulation

The forcing frequency of the load (ω) is situated in the range of natural frequency (ω_n) of the structure which resulted in the DAF value of 1.34. The DAF values of other two cases are larger than this case. Later, the reaction forces oscillate with the frequency of 6.2Hz which matches with the natural frequency of the structure as shown in *Table 4-1*.

The time history of vertical force acting on the cylinder and its corresponding response is shown in *Figure 4-19*. As observed in case 2 (*Figure 4-13*), here, the reaction force responds to some extent. This is because frequency of the slamming force is not so large compared to the natural frequency of the structure. The reaction force in negative direction is amplified with a DAF value of 1.45 approximately.

Figure 4-20 shows the horizontal and vertical deformation of the structural member. The displacement of the structural member is in the intermediate level of all three cases. The deformation curves follow the same trend as reaction forces with the frequency value of 6.2 Hz. The PSD graphs for two methods of coupling of this case are plotted in Appendix E.

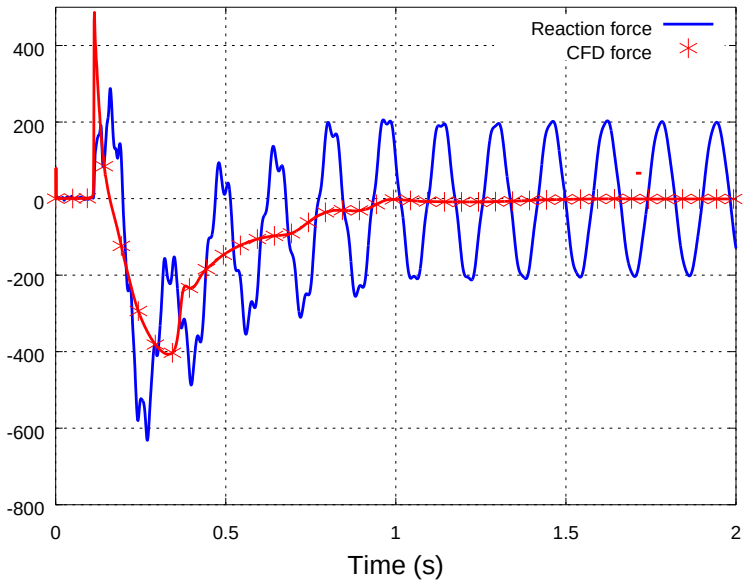

Figure 4-19 Vertical (CFD & Reaction) forces of case3 (one-way) coupling simulation

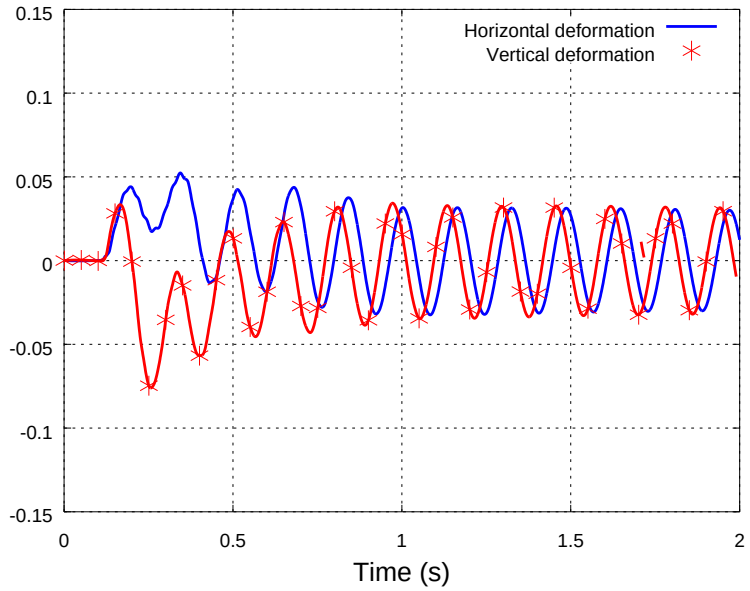

Figure 4-20 Horizontal and vertical deformation of the structural member- case3 (one-way)

4.8 Case3 (two-way)

Figure 4-21 shows the time history of CFD horizontal force (wave loads) and the reaction force (dynamic response) of the structural member for the two-way coupling simulation of case 3. The CFD force curve behaves in a different way compared to the one-way coupling. Here, the magnitude of reaction force is almost same as CFD force because the loads act in a different manner for two-way coupling method when damped by the surrounding water. After this, the reaction force continues to oscillate

with the natural frequency of the structure, but with the less magnitude due to damping.

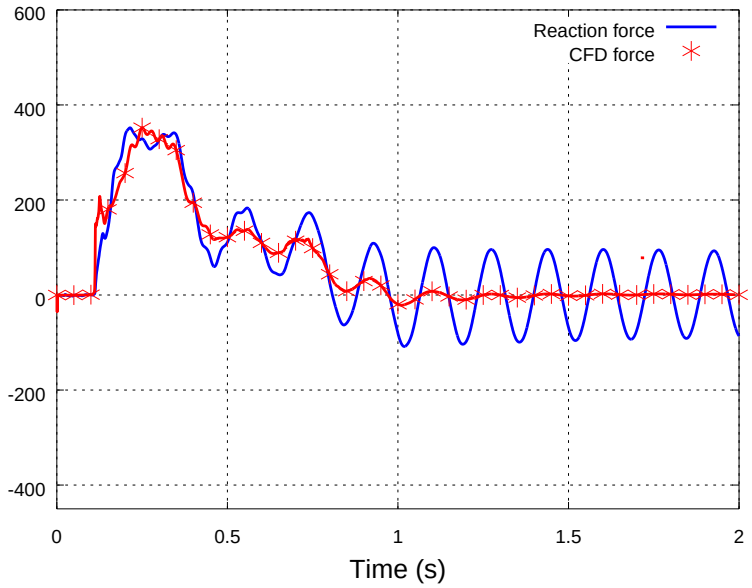

Figure 4-21 Horizontal (CFD & Reaction) forces of case3 (two-way) coupling simulation

The time history of vertical force acting on the cylinder and its corresponding response is shown in *Figure 4-22*. The difference between the magnitudes of peak vertical force among two methods of coupling is around 50kN which denotes that the structural member is less rigid to case 2, also, the dynamic amplification is smaller due to the behaviour of loads. An interesting result is that the reaction force is almost completely damped out from the time of 1s.

Figure 4-23 shows the deformation in both directions. The displacement of the structural member in both directions is virtually same as one-way coupling compared other two cases. At the time of 1s, the structural member stops to deform vertically whereas the horizontal deformation exists according to the dynamic response. The horizontal deformation curve repeats with frequency of 6.2Hz.

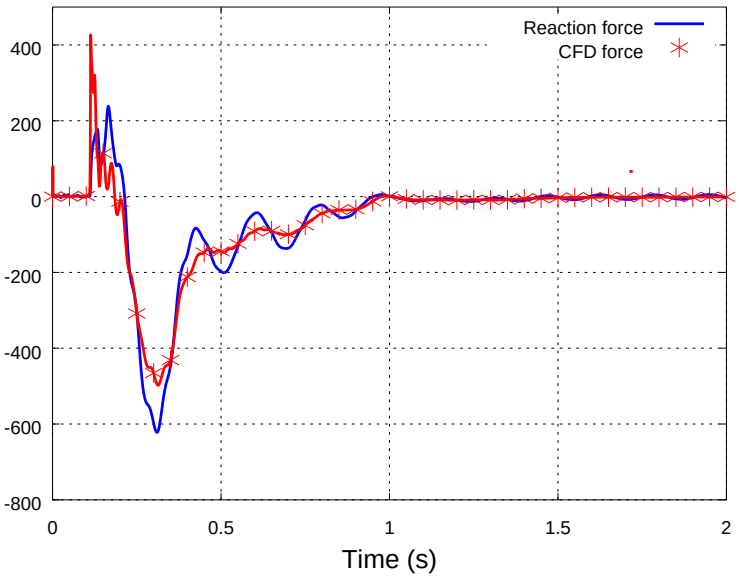

Figure 4-22Vertical (CFD & Reaction) forces of case3 (two-way) coupling simulation

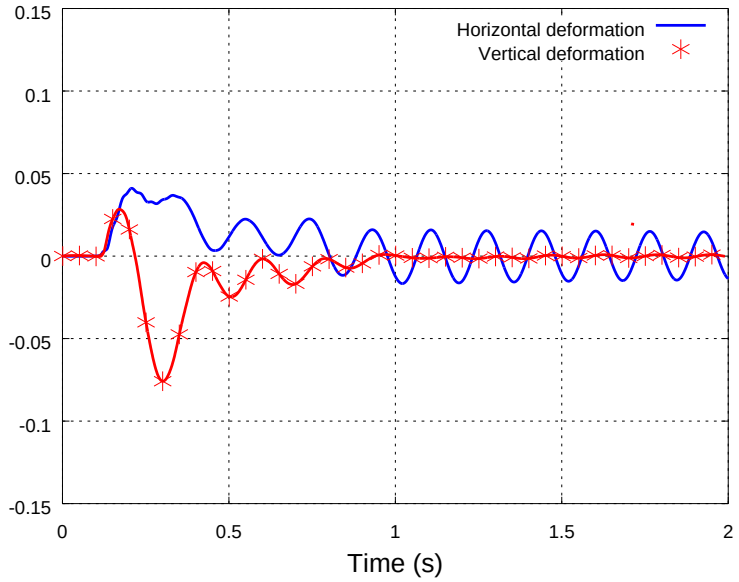

Figure 4-23 Horizontal and vertical deformation of the structural member- case3 (one-way)

4.9 Validation

Some very limited validation work of this project have been done by comparing the horizontal fluid force with the result of Morison equation and vertical CFD force with the experimental data presented by Isaacson and Prasad (1994) [22].

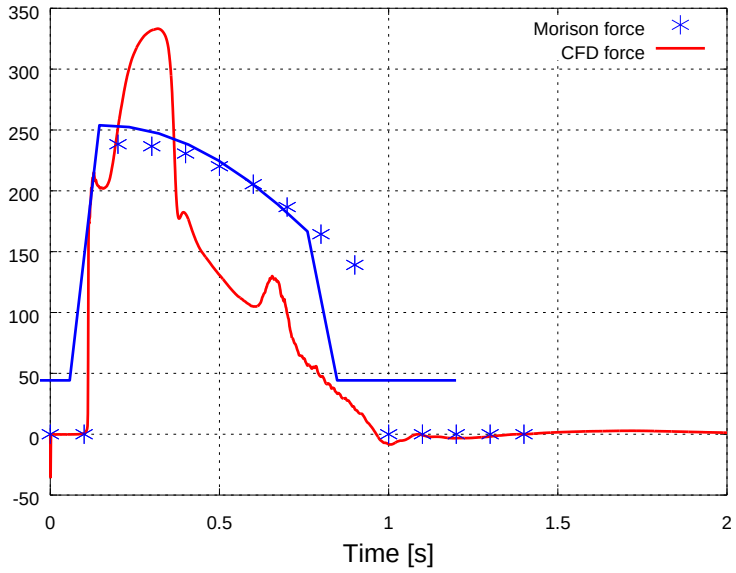

Figure 4-24 Validation of horizontal CFD fluid force

Figure 4-24 shows the comparison of horizontal fluid force attained by the numerical method with result of Morison equation. The formula mentioned in section 2.3.3 with C_M and C_D as 2.0 and 0.65 respectively is used to find horizontal force value. The difference between peak values of two curves is observed as 100 kN approximately. The reason for such difference is probably due to the fact that Morison equation cannot handle free surface effects.

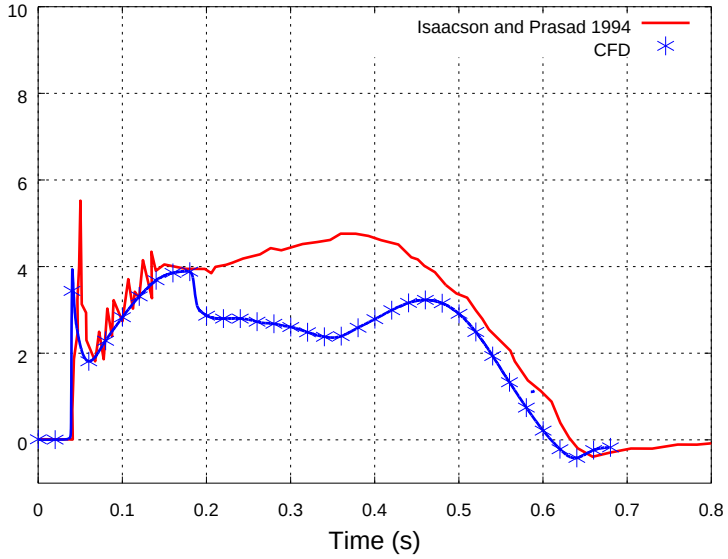

Figure 4-25 Validation of vertical CFD fluid force

Figure 4-25 depicts the comparison of vertical force curves; the CFD force curve is obtained by using the fluid model which is similar to the model of this project. The CFD model used in validation follows the same meshing and simulation strategies of the fluid model of current work. But the flow is treated as a laminar flow because of the low Reynolds number in the scaled model test. The critical point of this validation is that the comparison has been done between the wave forces and the reaction forces measured from the experiment. Due to dynamic amplification, the reaction forces are potentially amplified which are measured using dynamometers and this is the reason for such a difference between the peak vertical forces (slamming force). Other differences may be related to the simulated Stokes 5^{th} order wave differs from the real wave in the flume test.

As described in section 2.3.4, the initial vertical force peak can be described by a slamming coefficient *Cs.* Many experimental studies had been conducted to establish appropriate values of maximum slamming coefficient for a case of circular cylinder and numerical models are developed with those coefficients in order to determine the time history of vertical force. The results of tests with different wave periods and heights and with different cylinder elevations exhibit the maximum slamming coefficient mean values which range from 3.04 to 7.79 [23].

A comparison of slamming coefficients derived from the FSI analyses performed in this project, see ***Table 4-2***, is made with the coefficients reported in [23].

Table 4-2 Evaluation of slamming coefficient for both CFD and reaction forces

	Fs (N)	**Cs_F**	**Reaction force(N)**	**Cs_R**
One-way				
Case-1	481250	11.68	120750	2.93
Case-2	481250	11.68	410590	9.97
Case-3	481250	12.08	291625	7.08
Two-way				
Case-1	369850	8.98	109560	2.66
Case-2	445200	10.81	364810	8.86
Case-3	430800	10.46	245840	5.97

The coefficient values (Cs_F) of fluid forces are not scattering as the coefficient values (Cs_R) of reaction forces and this is because of the dynamic amplification of reaction forces in different cases. Also, it is clear to notice that slamming coefficient values (Cs_R) determined from numerical reaction forces are nearly situated in the range of values provided by experimental studies.

5 Conclusions

The FSI analysis has been carried out on a horizontal slender cylindrical member with typical offshore dimensions placed above the free surface of the water in order to evaluate the effects of a wave fluid structure interaction. The work is performed by following two methods of coupling i.e. one-way coupling and two-way coupling. This is implemented by creating a large domain in which the structural member is placed in an appropriate position such that the wave impacts the member in a relatively short period of time in order to minimize analysis time. Fifth order Stokes wave theory is applied in the numerical wave modelling to simulate a high amplitude non-linear wave. The wave loads are numerically computed by creating the fluid model with help of ANSYS Fluent and the dynamic response of the structural model is extracted using ANSYS Mechanical. The exchange of these two solutions has been done by utilizing System Coupling in ANSYS Workbench.

Complete FSI analyses have been performed for three different cases of the structure with different material properties (different Young's modulus and material thicknesses) for the purpose of reaching the objectives of the project as mentioned in section 1.3. The CFD (wave loads) forces acting in both vertical and horizontal directions are plotted with its corresponding reaction forces extracted from the structural member. The structural responses of all three cases vary between the two methods of coupling. The DAF values of the one-way coupling are quite high compared to the two-way coupling simulations especially the high difference is noticed in case1. The reason for this difference is due to the behaviour of loading in the two-way coupling method i.e. the system is reduced to a good extent due to the existence of fluid damping. The horizontal fluid forces of three cases have very less variations between two methods of coupling. On other hand the values of vertical force have a reasonable difference in all three cases. This variation indicates the rigidity of structure in each case.

Finally, the main limitation of one-way coupling method seems to be that the effect of water acting as a damper is neglected which leads to the dynamic amplification in all three cases. Also, it is observed that the structural member's response is matching with its respective natural frequencies which are evident from PSD plots.

6 Future work

In this project work, the length and diameter of the member is considered as 20m and 0.8m respectively for three different cases of the structure as shown in

Table 3-3. Therefore, all six analyses have been done with these dimensions, but it could be interesting to do analyses with different dimensions. The current problem is comprised of only one inundation, so it is really motivating to do analyses with more than one inundation and different wave strengths. The results of this kind of analyses would be useful to verify conclusions of this project especially the consequence of fluid damping in two-way coupling method.

The next important recommendation for the future work of this project is to perform an analysis by one-way coupling method with the inclusion of structural damping. This will lead to saving of a big amount of computational efforts and resources if the results are as good as two-way coupling method. As a final point, this is kind of complex analysis would be much more helpful if it is able to solve with improved solver speed and high performance clusters.

Appendix

A. Wave theory coefficients

The coefficients used in the equation (2-14) are described below. The terms c_h and s_h are the representation of *cosh (kh)* and *sinh (kh)* respectively.

$$B_{22} = \frac{(2c_h^2 + 1)c_h}{4s_h^3}$$

$$B_{24} = \frac{(272\ c_h^8 - 504\ c_h^6 - 192\ c_h^4 + 322\ c_h^2 + 21)c_h}{384\ s_h^9}$$

$$B_{33} = \frac{3(8c_h^6 + 1)}{64\ s_h^6}$$

$$B_{35} = \frac{88128\ \ c_h^{14} - 208224\ \ c_h^{12} + 70848\ \ c_h^{10} + 54000\ \ c_h^8 - 21816\ \ c_h^6 + 6264\ \ c_h^4 - 54\,c_h^2 - 81}{12288\ \ s_h^{12}\,(6c_h^2 - 1)}$$

$$B_{44} = \frac{(768\ c_h^{10} - 448\ c_h^8 - 48\,c_h^6 + 48\,c_h^4 + 106\ c_h^2 - 21\ )c_h}{384\ s_h^9\,(6c_h^2 - 1)}$$

$$B_{55} = \frac{192000\ \ c_h^{16} - 262720\ \ c_h^{14} + 83680\ \ c_h^{12} + 20160\ \ c_h^{10} - 7280\ \ c_h^8 + 7160\ \ c_h^6 - 1800\ \ c_h^4 - 1050\ \ c_h^2 + 225}{12288\ \ s_h^{10}\,(6c_h^2 - 1)(8c_h^4 - 11c_h^2 + 3)}$$

As mentioned in section 2.3.2 , the value of coefficients $C_1$and C_2 are expressed below

$$C_1 = \frac{8c_h^4 - 8c_h^2 + 9}{8s_h^4}$$

$$C_2 = \frac{3840\ \ c_h^{12} - 4096\ \ c_h^{10} + 2592\ \ c_h^8 - 1008\ \ c_h^6 + 5944\ \ c_h^4 - 1830\ \ c_h^2 - 147}{512\ \ s_h^{10}\,(6c_h^2 - 1)}$$

The coefficients used in the equations of velocity (2-17 and 2-18) are given as

$$A_{11} = \frac{1}{s_h}$$

$$A_{13} = -\frac{c_h^2\,(5c_h^2 + 1)}{8s_h^5}$$

$$A_{15} = -\frac{1184\ c_h^{10} - 1440\ c_h^{8} - 1992\ c_h^{6} + 2641\ c_h^{4} - 249\ c_h^{2} + 18}{1536\ s_h^{11}}$$

$$A_{22} = \frac{3}{8 s_h^{4}}$$

$$A_{24} = \frac{192\ c_h^{8} - 424\ c_h^{6} - 312\ c_h^{4} + 480\ c_h^{2} - 17}{768\ s_h^{9}}$$

$$A_{33} = \frac{13 - 4 c_h^{2}}{64\ s_h^{7}}$$

$$A_{35} = \frac{512\ c_h^{12} + 4224\ c_h^{10} - 6800\ c_h^{8} - 12808\ c_h^{6} + 16704\ c_h^{4} - 3154\ c_h^{2} + 107}{4096\ s_h^{13} (6 c_h^{2} - 1)}$$

$$A_{55} = -\frac{2880\ c_h^{10} - 72480\ c_h^{8} + 324000\ c_h^{6} - 432000\ c_h^{4} + 163470\ c_h^{2} - 16245}{61440\ s_h^{11} (6 c_h^{2} - 1)(8 c_h^{4} - 11 c_h^{2} + 3)}$$

$$A_{44} = \frac{80 c_h^{6} - 816\ c_h^{4} + 1338\ c_h^{2} - 197}{1536\ s_h^{10} (6 c_h^{2} - 1)}$$

B. Velocity variation inside a boundary layer

The below x-y plot shows the velocity variation of water particles along a vertical line above the surface of the cylinder. This variation occurs at the time of 0.5 s.

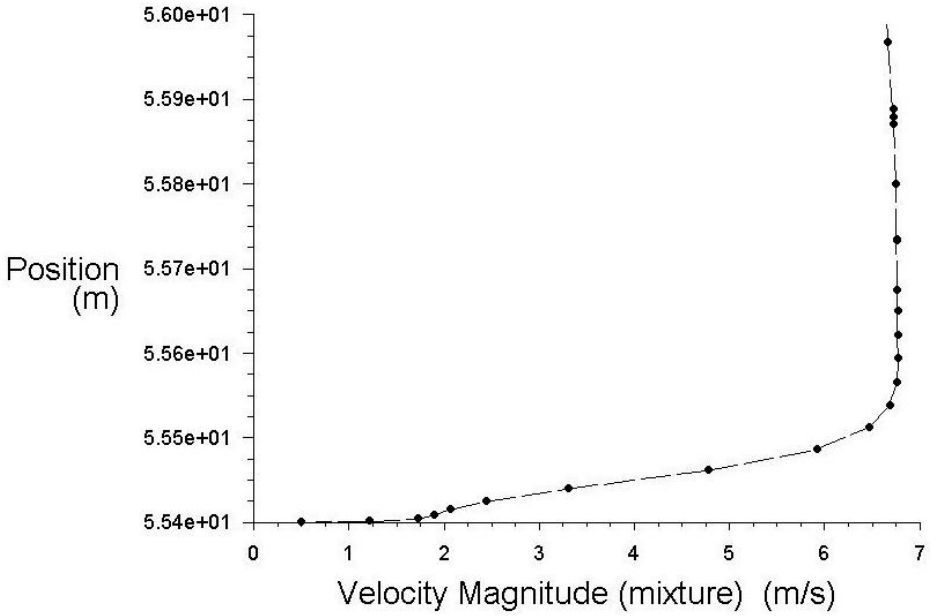

Figure B-1 Velocity variation along a vertical line above the surface of the structural member

This plot is taken for the purpose of knowing the velocity variation inside the boundary layer of the flow. Initially, numerical calculation has been done with a simple mesh resolution around the structural member. Then with the help of Fluent the above plot has been drawn in order to find an approximate boundary layer thickness. The approximate boundary layer thickness appears to be double the diameter of a structural member. For this reason, a larger cylinder of diameter 0.8m has been created so that the mesh resolution can be done in a better way in order to resolve the boundary layer and this plot is drawn before conducting a mesh convergence study.

C. Analytical calculation of deformation of a cylinder

An analytical method of calculating the deformation of a structural member has been done before the numerical simulation in order to get a rough estimate about the deflection values. This calculation is performed by considering a beam fixed at both ends with uniform distributed load. The formula for calculating the deflection at center of a beam for this case is given as

$$\delta_{\max}(center) = \frac{wl^4}{384\,EI}$$

$$I = \frac{\pi}{64}\left(d_2^4 - d_1^4\right)$$

where I is moment of inertia of a circular cylinder of thickness (t), d_2 and d_1 are the outer and inner diameters of a cylinder respectively, E is the Young's modulus of a beam, w (N/m) is the load acting on a unit length of a beam and l is the length of a beam.

Initially, the moment of inertia of a circular cylinder with different thickness have been listed in the below table.

Table C -1 Moment of inertia of cylinder with different thickness

d_2(m)	t(m)	d_1(m)	I(m^4)
0.8	0.0025	0.7950	0.000497962
0.8	0.0050	0.7900	0.000986617
0.8	0.0075	0.7850	0.001466081
0.8	0.0100	0.7800	0.00193647
0.8	0.0125	0.7750	0.0023979
0.8	0.0150	0.7700	0.002850484
0.8	0.0200	0.7600	0.003729573
0.8	0.0250	0.7500	0.004574638
0.8	0.0300	0.7400	0.005386567
0.8	0.0400	0.7200	0.00691452

In order to find a load per unit length (w), the peak value of CFD horizontal force (334 kN approximately) is used. This value is divided by the length of the structural member. This calculation is performed for a large number of cases varying the thickness and Young's modulus of a beam which is shown in *Table C-2*.

Table C-2 Matrix containing the deflection values for varying E (Pa) and t (mm)

	Deflection δ(m)						
t(m)/E(Pa)	**2.00E+09**	**3.00E+09**	**5.00E+09**	**1.00E+10**	**2.00E+10**	**5.00E+10**	**2.00E+11**
0.0025	6.98388	4.65592	2.79355	1.39678	0.69839	0.27936	0.06984
0.0050	3.52488	2.34992	1.40995	0.70498	0.35249	0.14100	0.03525
0.0075	2.37211	1.58141	0.94885	0.47442	0.23721	0.09488	0.02372
0.0100	1.79590	1.19727	0.71836	0.35918	0.17959	0.07184	0.01796
0.0125	1.45031	0.96688	0.58013	0.29006	0.14503	0.05801	0.01450
0.0150	1.22004	0.81336	0.48802	0.24401	0.12200	0.04880	0.01220
0.0200	0.93247	0.62165	0.37299	0.18649	0.09325	0.03730	0.00932
0.0250	0.76022	0.50681	0.30409	0.15204	0.07602	0.03041	0.00760
0.0300	0.64563	0.43042	0.25825	0.12913	0.06456	0.02583	0.00646
0.0400	0.50296	0.33530	0.20118	0.10059	0.05030	0.02012	0.00503

One of the main objectives of this FSI analysis is to evaluate the significance of both the ways of coupling under various conditions of deflection of a beam. So, with the aim to have a reasonable conclusion form the work the three different cases from the above table is chosen which is shown in section 3.3.

D. Stress concentration of a structural member

Below figures show the Von Mises equivalent stress of the structural member for case 1, case 2 and case 3. This is measured with respect to a single point located at the centre of the cylinder. In general, all curves are following the same pattern as its reaction forces which are shown in section 4. The highest value of stress concentration of around 8 MPa is observed in case 1 because of its large deformation compared to other cases. On other hand, the peak values of other two cases are noticed as 4 MPa approximately. Although the peak value of case 2 and case 3 are almost similar, the stress concentration at the later stages i.e. when water passed over the structural member, have a big difference. The main observation of these plots is considered as the difference of stress concentration values between one-way and two-way coupling methods. Due to fluid damping in two-way simulations, stress concentrations are limited to a good extent.

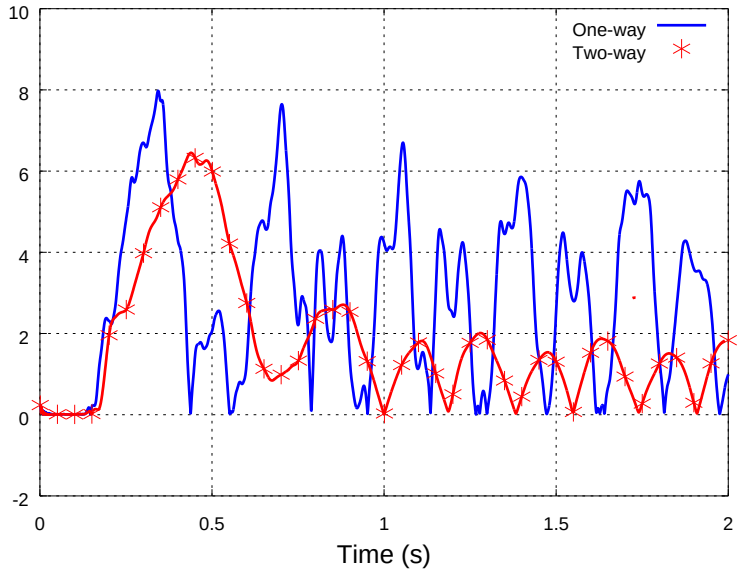

Figure D-1 Stress concentration for case 1

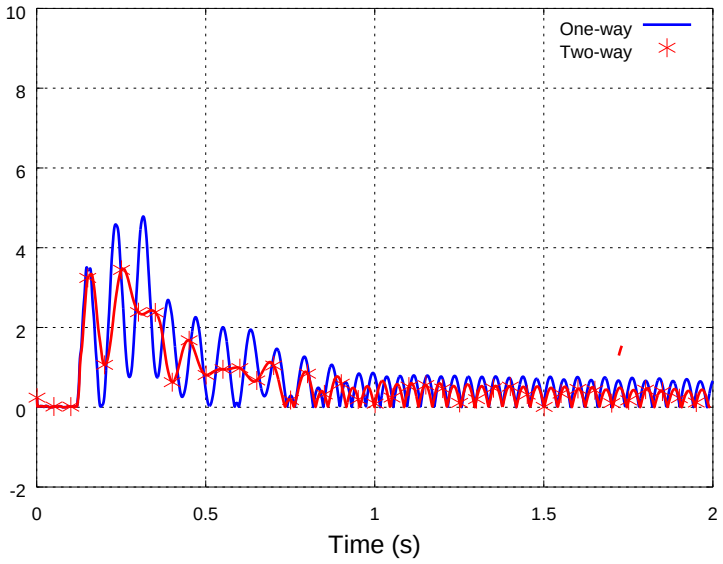

Figure D-2 Stress concentration for case 2

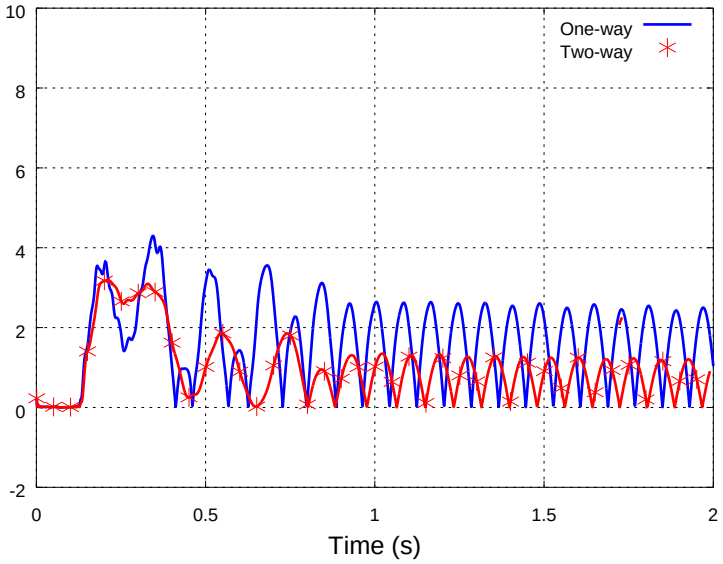

Figure D-3 Stress concentration for case 3

E. Power spectral density graphs

This section of the report contains the PSD plots for all six different cases of simulations. Generally, this analysis is performed to understand the strength of a signal in the frequency domain. Here, the displacement value of each case is used in plotting PSD graphs.

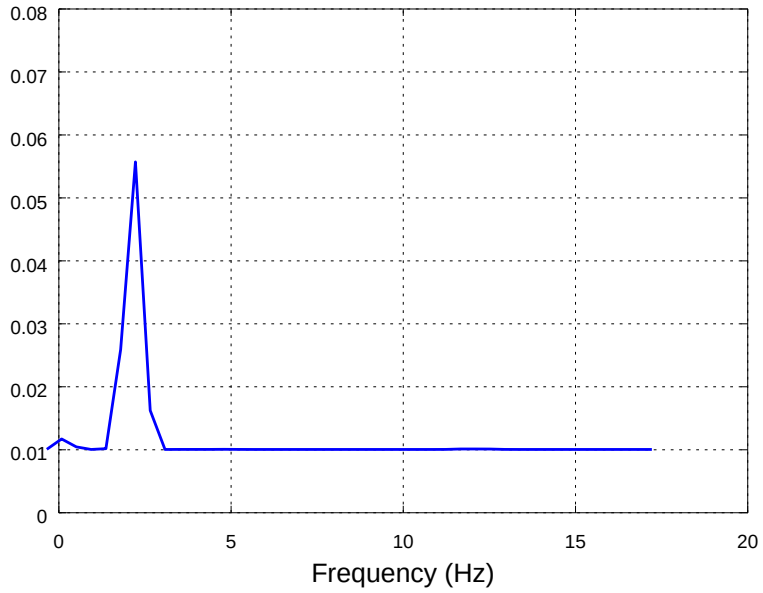

Figure E-1 PSD graph of case 1(one-way)

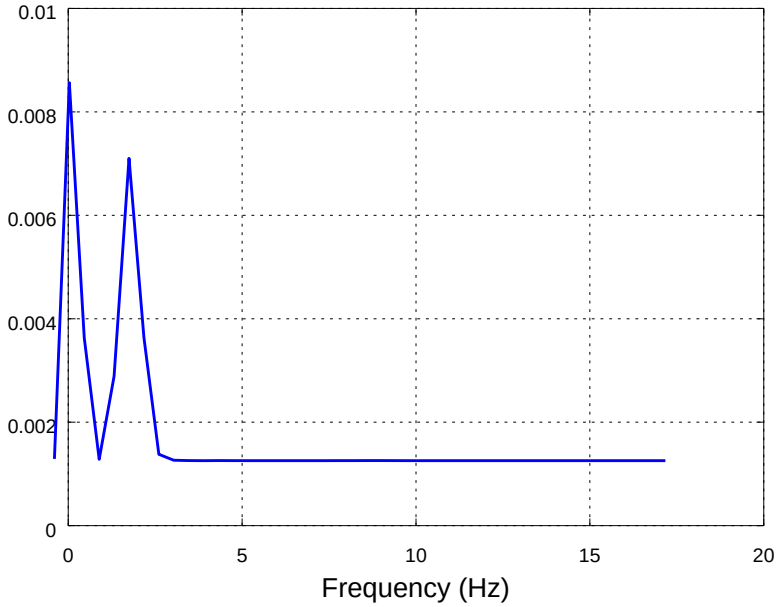

Figure E-2 PSD graph of case 1(two-way)

Figures show the frequency spectrum for two different methods (one-way and two-way) of simulations of case 1. In the case of one-way coupling method, the mean frequency of spectrum is considered as the first natural frequency of the structural member which is shown in *Table 4-1*. But in two-way simulation, other than the natural frequency of the member, one more peak is noted at the value of around 0.5 Hz which seems to be the wave loading frequency.

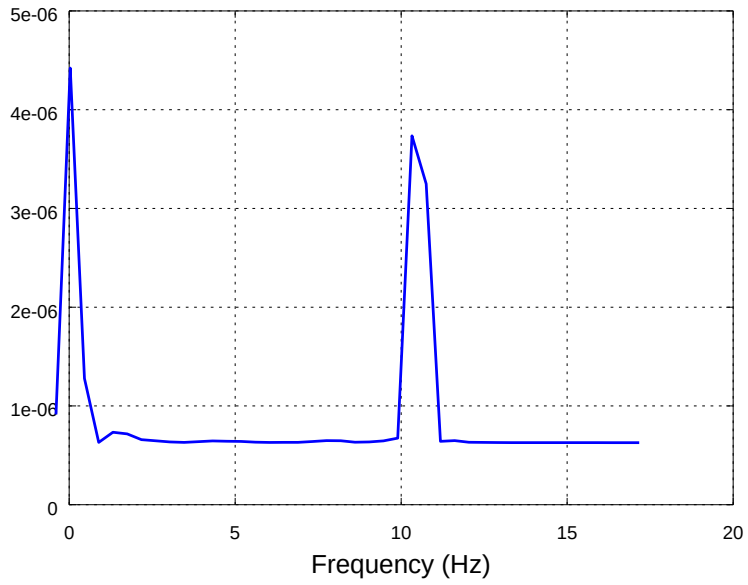

Figure E-3 PSD graph of case 2(one-way)

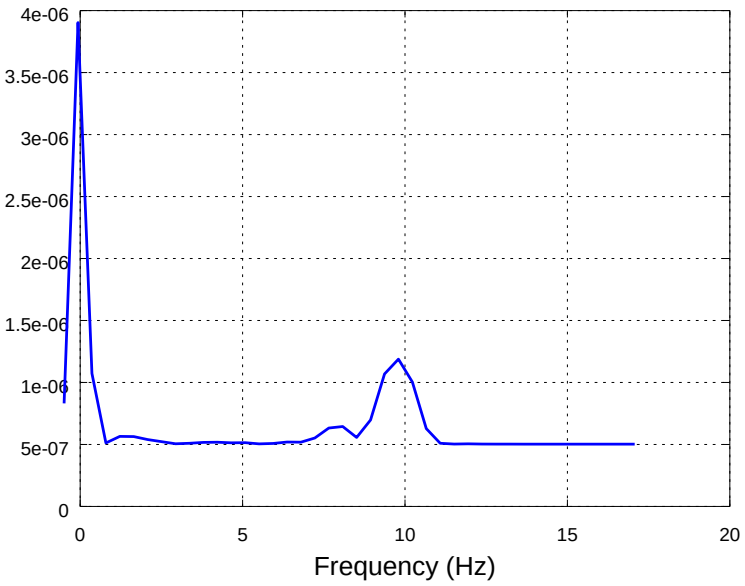

Figure E-4 PSD graph of case 2(two-way)

Figures show the frequency spectrum of one-way and two-way simulations of case 2 respectively. The oscillating frequency of the structure of this case is observed as the first natural frequency of around 12.5 Hz as given in *Table 4-1*. Also, the wave loading frequency of 0.5 Hz is dominated with a large magnitude in two different methods of simulation.

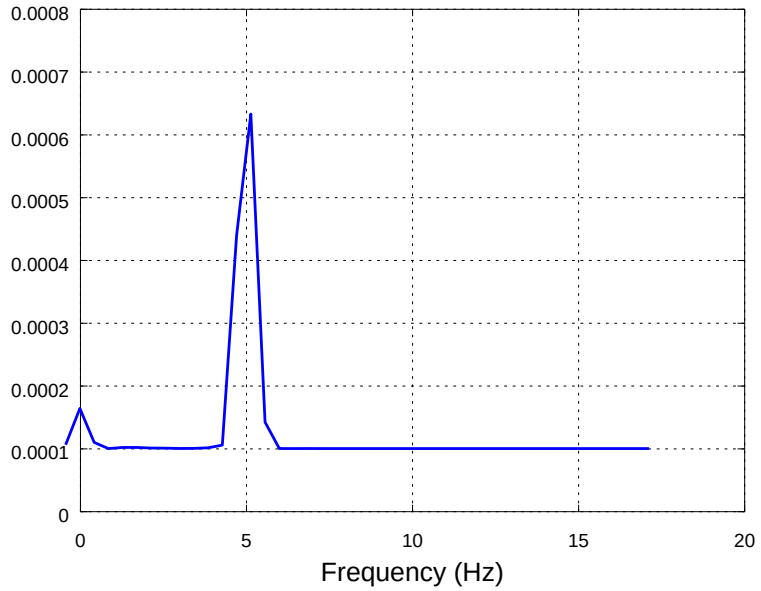

Figure E-5 PSD graph of case 3(one-way)

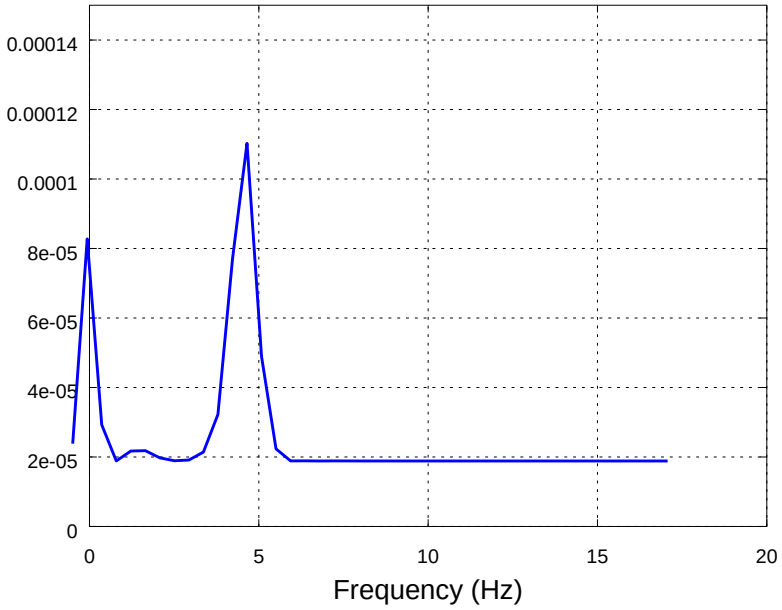

Figure E-6 PSD graph of case 3(two-way)

The PSD plots of two methods of coupling of case 3 are shown in figures. It is clear to notice that the mean frequency of spectrum is same as the natural frequency of the structural member which is given in *Table 4-1*. The loading frequency of around 0.5 Hz is also observed in this case to a good extent.

References

1. B.Iwanowski, R.Gladso, M.Lefranc, "Wave-in-deck load on a jacket platform, CFD derived pressures and non- linear structural response" *28th OMAE International conference, Hawaii, USA.* May 31- June 5, 2009.

2. A.K.Pozarlik, J.B.W.Kok, "Numerical investigation of one-way and two-way fluid structure interaction in combustion systems" *International conference on computational methods for coupled problems in Science and Engineering, Barcelona.*2007.

3. *ANSA 13.2.1* BETA CAE Systems S.A. P.O. Box 18623, GR-54005 Thessaloniki, Greece

4. *Fluent 14.0.* ANSYS, Inc., Southpointe, 275 Technology Drive, Canonsburg, PA15317, USA.

5. Z.Yun, Y.Hui, "Coupled fluid structure flutter analysis of a transonic fan" *Chinese Journal of Aeronautics,* vol.24, 2011, 258-264.

6. S.A.Anagnostopoulos, "Dynamic response of offshore platforms to extreme waves including fluid structure interaction" *Eng.Struct.,*vol. 4, July, 1982.

7. G.Dubini, R.Pietrabissa, F.M.Montevecchi "Fluid structure interaction problems in bio-fluid mechanics: a numerical study of the motion of an isolated particle freely suspended in channel flow" *Med.Eng.Phys,* vol.17, 1985, 609-617.

8. S.K Chakrabarti, "*Handbook of offshore engineering*" Elsevier, 1st ed., 2005.

9. F.Vikebo, T.Furevik, G.Furnes, N.G.Kvamsto, M.Reistad, "Wave height variations in the North Sea and on the Norwegian Continental Shelf, 1881-1999"*Continenetal Shelf Research*, vol.23, 2003, 251-263.

10. K.v.Raaij "Dynamic behaviour of jackets exposed to wave-in-deck forces" Ph D thesis, University of Stavanger, Norway (2005).

11. R.G.Bea, T.Xu, J.Stear, R.Ramos, "Wave forces on decks of offshore platforms" *Journal of waterway, port, coastal and ocean Engineering*, 1999.

12. T.Richter, "Numerical methods for fluid–structure interaction problems" 2010.

13. G.Hou, J.Wang, A.Layton , " Numericalmethods for fluid structure interaction- A review" *Commun.Comput.Phys,* vol.12 , no. 2, 2012, 337-377.

14. F.K. Benra, H.J.Dohmen, J.pei, S.Schuster, B.Wan, "A comparison of one-way and two-way coupling methods for numerical analysis of fluid structure interactions" *Journal of applied mathematics,* ID 853560, 2011.

15. H.Versteeg, W.Malalasekra, "An introduction to computational fluid dynamics" Pearson Prentice Hall, 2nd ed., 2007.

16. *ANSYS Workbench 14.0*- user guide

17. L.Davidson, "An Introduction to turbulence models". Course material. 2003.

18. V.R.Gopala, G.M. van Wachem, "Volume of fluid methods for immiscible-fluid and free syrface flows" *Journal of Chemical engineering,* vol. 141, 2008, 204-221.

19. A.K.Chopra "Dynamics of structures" Pearson Prentice Hall, 2nd ed., 2001.

20. P.Lin, "Numerical modelling of water waves" Taylor and Francis, 1st ed., 2008.

21. J.D Fenton, "Nonlinear wave theories" *The sea, vol. 9 Ocean Engineering science.*

22. S. Prasad, "Wave impact forces on a Horizontal cylinder", PhD thesis, The University of British Columbia, Canada 1994.

23. M.Isaacson, S. Prasad, "Wave slamming on a Horizontal circular cylinder" *International journal of offshore and polar Engineering*, vol.4,no.2, 1994.

24. http://www.oas.org/cdcm_train/courses/course21/chap_05.pdf

25. http://www.cfd-online.com/Tools/yplus.php